
**Pacific Northwest
National Laboratory**

Operated by Battelle for the
U.S. Department of Energy

Mineral Identification of Geologic Samples from Borehole C4998

J. V. Crum
B. J. Riley

November 2006

Work performed for the Office of River Protection under
Project Number 49647
Prepared for the U.S. Department of Energy
under Contract DE-AC06-76RL01830



DISCLAIMER

This report was prepared as an account of work sponsored by an agency of the United States Government. Neither the United States Government nor any agency thereof, nor Battelle Memorial Institute, nor any of their employees, makes **any warranty, express or implied, or assumes any legal liability or responsibility for the accuracy, completeness, or usefulness of any information, apparatus, product, or process disclosed, or represents that its use would not infringe privately owned rights.** Reference herein to any specific commercial product, process, or service by trade name, trademark, manufacturer, or otherwise does not necessarily constitute or imply its endorsement, recommendation, or favoring by the United States Government or any agency thereof, or Battelle Memorial Institute. The views and opinions of authors expressed herein do not necessarily state or reflect those of the United States Government or any agency thereof.

PACIFIC NORTHWEST NATIONAL LABORATORY
operated by
BATTELLE
for the
UNITED STATES DEPARTMENT OF ENERGY
under Contract DE-ACO5-76RL01830

Printed in the United States of America

**Available to DOE and DOE contractors from the
Office of Scientific and Technical Information,
P.O. Box 62, Oak Ridge, TN 37831-0062;
ph: (865) 576-8401
fax: (865) 576 5728
email: reports@adonis.osti.gov**

**Available to the public from the National Technical Information Service,
U.S. Department of Commerce, 5285 Port Royal Rd., Springfield, VA 22161
ph: (800) 553-6847
fax: (703) 605-6900
email: orders@nits.fedworld.gov
online ordering: <http://www.ntis.gov/ordering.htm>**

Mineral Identification of Geologic Samples from Borehole C4998

J. V. Crum
B. J. Riley

November 2006

Work performed for the Office of River Protection
under Project Number 49647

Prepared for the U.S. Department of Energy
under Contract DE-AC05-76RL01830

Pacific Northwest National Laboratory
Richland, Washington 99352

Summary

Samples taken from borehole C4998 at the Waste Treatment Plant (WTP) on the Hanford Site in southeastern Washington State were characterized to help determine secondary minerals within the basalt formations below the site. These analyses were performed to provide supplemental qualitative characterization information on basalt samples from below the WTP. The analytical data has been determined to be non-quality affecting. Therefore, PNNL standard laboratory practices and procedures were used. The samples were analyzed with X-ray diffraction, and the measured diffraction patterns for unknown samples were matched with indexed diffraction patterns in the databases. Search-match software was used to select the best match from the International Center for Diffraction Data mineral database or the Inorganic Crystal Structure Database based on peak locations and intensities. Clays were identified in 81% and plagioclase in 49% of the samples. Quartz was identified in 24% and pyroxene in 16% of the samples. The carbonates, siderite and rhodochrosite, were identified in 16% of the samples. Rhodochrosite was identified in only one sample. Siderite was the major phase in 67% of the samples and once each as a minor and trace phase in samples that contained siderite. Zeolite was identified as the major phase in 11% of the samples at three locations. A few samples contained minerals different than those seen from the many fractures sampled. These minerals were cristobalite, hematite, opal, pyrite, tridymite, and vaesite. The data obtained from this work are useful to help characterize the mineralogy within the fractures of the basalts.

Abbreviations

DBS	Depth below surface
PDF	Powder diffraction file
WTP	Waste Treatment Plant
XRD	X-ray diffraction

Contents

Summary	iii
Abbreviations and Acronyms	v
1.0 Introduction.....	1.1
2.0 Experimental Method	2.3
3.0 Results.....	3.5
4.0 References.....	4.9
Appendix A: XRD Patterns Showing Chemical Composition of Minerals	A.1

Figures

3.1. Comparing the Clay at 642 ft with and Without Ethylene Glycol Treatment	3.5
A.1. XRD Pattern for Sample 518-A	A.1
A.2. XRD Pattern for Sample 518-B	A.2
A.3. XRD Pattern for Sample 519.1	A.3
A.4. XRD Pattern for Sample 559.5-A	A.4
A.5. XRD Pattern for Sample 559.5-B	A.5
A.6. XRD Pattern for Sample 561.0	A.6
A.7. XRD Pattern for Sample 631.5	A.7
A.8. XRD Pattern for Sample 642	A.8
A.9. XRD Pattern for Sample 653.3	A.9
A.10. XRD Pattern for Sample 673-A	A.10
A.11. XRD Pattern for Sample 673-B	A.11
A.12. XRD Pattern for Sample 714.2	A.12
A.13. XRD Pattern for Sample 778.6	A.13
A.14. XRD Pattern for Sample 815	A.14
A.15. XRD Pattern for Sample 954.4-A	A.15
A.16. XRD Pattern for Sample 954.4-B	A.16
A.17. XRD Pattern for Sample 964	A.17
A.18. XRD Pattern for Sample 992	A.18
A.19. XRD Pattern for Sample 1020-A	A.19

A.20. XRD Pattern for Sample 1020-B	A.20
A.21. XRD Pattern for Sample 1043.8	A.21
A.22. XRD Pattern for Sample 1060.6	A.22
A.23. XRD Pattern for Sample 1090.3	A.23
A.24. XRD Pattern for Sample 1090.3-B	A.24
A.25. XRD Pattern for Sample 1208.6	A.25
A.26. XRD Pattern for Sample 1213.3	A.26
A.27. XRD Pattern for Sample 1219	A.27
A.28. XRD Pattern for Sample 1231.5	A.28
A.29. XRD Pattern for Sample 1231.6	A.29
A.30. XRD Pattern for Sample 1233.8	A.30
A.31. XRD Pattern for Sample 1241.5	A.31
A.32. XRD Pattern for Sample 1266.2	A.32
A.33. XRD Pattern for Sample 1267	A.33
A.34. XRD Pattern for Sample 1269	A.34
A.35. XRD Pattern for Sample 1277.5	A.35
A.36. XRD Pattern for Sample 1360.7	A.36
A.37. XRD Pattern for Sample 1375.5	A.37

Table

2.1. Sample Mineralogy as a Function of Depth Below the Surface (DBS).....	2.4
--	-----

1.0 Introduction

This report documents secondary mineral-identification results obtained by X-ray diffraction (XRD) analysis of samples taken from borehole C4998 drilled at the Waste Treatment Plant (WTP) on the Hanford Site (PNNL 2006). These analyses were performed to provide supplemental qualitative characterization information on basalt samples from below the WTP. The analysis data have been determined to be non-quality affecting; therefore, PNNL standard laboratory practices and procedures were used.

2.0 Experimental Method

The following steps were taken to prepare each sample for analysis by XRD. First, each sample was ground to a very fine powder using an agate mortar and pestle. Second, depending upon the amount of available powder, the samples were either packed into a cavity or coated onto the flat surface on the backside of the XRD sample holder. The holder used was a zero-background quartz slide with a 10-mm-diameter cavity, cut from a single crystal of quartz. It was cut off axis such that it would not produce any peaks in the scanning process. Third, XRD measurements were performed with a Scintag PAD V diffractometer using Cu K α radiation ($\lambda = 1.5406 \text{ \AA}$, 45 kV, and 40 mA) and equipped with a Peltier-cooled Si(Li) solid-state detector. The experiments were done using $\theta - 2\theta$ geometry in a step-scan approach from 2° to $50^\circ 2\theta$ with a step size of $0.04^\circ 2\theta$ and a dwell time of 4 seconds per step. Jade 6[®] software was used to process and identify phase assemblages from the International Center for Diffraction Data and Inorganic Crystal Structure Database mineral databases. The best match was selected based on peak locations and intensities.

One sample, 642 ft, was analyzed using the following clay mount method. This method consists of first placing approximately 2 g of fine powder into a scintillation vial filled with deionized water. Next, an ultrasonic probe was placed into the scintillation vial to separate agglomerated clay particles. Following sonication, the vial was left undisturbed for 2 hours to allow settling of all particles greater in size than clays. Then, a small aliquot was pipetted from the top of the scintillation vial, pipetted onto an XRD slide, and allowed to dry overnight. The sample was scanned using the same conditions given above. Then, the sample was exposed to an ethylene glycol atmosphere to promote expansion. The sample was then rescanned to detect peak shifts related to clay expansion. The clay analysis method described above was modified from the procedure described by Moore and Reynolds (1989).

Table 2.1. Sample Mineralogy as a Function of Depth Below Surface (DBS)

Sample ID/DBS (ft)	Sample Mounting ^(a)	Description (from Geologist's Log)	Minerals Identified by XRD ^(b,c)						
			Quartz	Plagioclase	Pyroxene	Siderite	Zeolite	Clays 12-15 Å	Other Phases ^c
518.0A	P	Sickened sides/fracture fill		T				X	
518.0B	C	Sickened sides/fracture fill		T				X	
519.1	p	White powder	T	T					Op
559.5A	P	Black crystals		O				X	
559.5B	P	Black crystals		T				X	
561.0	P	Chalcedony							C, T
631.5	P	Fracture fill		T	T			X	
642	P	Fracture fill						X	
653.3	P	Sickened sides/fracture fill						X	
673A	P	Green fracture fill			T			X	
673B	P	Black fracture fill		X	T			O	
714.2	C	Fracture fill		T				X	
778.6	C	Black fracture fill		T				X	
815	C	Black fracture fill		T				X	
954.4A	P	Vesicle filler				X			R
954.4B	P	Sulfide mineral							Py, V
964	P	Fracture fill					X	O	
992	P	Black fracture fill						X	
1020A	P	Clear encrusting crystals					X	O	
1020B	C	Green clay						X	
1043.8	P	Breccia matrix		X	T			O	
1060.6	C	Low angle fracture fill		T				X	
1090.3A	P	Clear crystals in fracture fill					X		
1090.3B	C	Black botryoidal mineral					T	X	H
1208.6	P	Vvg coating				T		X	
1213.3	P	Brown/green cavity lining		T		X		O	
1219	C	Green/brown fracture fill	X			O		T	
1231.5	P	Top edge of cumulate chamber	O	T		X			
1231.6	P	Vesicle		O	T			X	
1233.8	C	Green fracture fill		O		X		T	
1241.5	P	White fracture fill	X						
1266.2	P	Green fracture fill	T	T				X	
1267	P	Green/brown fracture fill	X					T	
1269	P	Brown fracture fill	X					T	
1277.5	P	N/A	X					O	
1360.7	P	N/A	O					X	
1375.5	P	N/A		O	T			X	

(a) P=cavity packed; C=surface coated
(b) X=major phase; O=minor phase; T=trace amounts
(c) C=cristobalite; H=hematite; Op=opal; Py=pyrite; R=rhodochrosite; T=tridymite; V=vaesite

3.0 Results

Identified phases, relative concentrations, sample description from the field, and the DBS are given in Table 2.1. The results for all 37 samples are arranged by depth below the surface, from 518 ft below the surface to a maximum depth of 1375 ft. The major phases identified listed according to abundance were clays, plagioclase, quartz, pyroxene, siderite, zeolite, and in one sample, pyrite.

Clays (12-15 Å) were identified in 81% of the samples measured. Clay was the major phase in 67%, the minor phase in 20%, and a trace phase in 13% of the samples containing clays. It is present at almost all depths within the range of depths measured. In Table 2.1, the identification of clays has been generically categorized by the location of the first diffraction peak in terms of d-spacing. The 12-15 Å clays identified could be a smectite based on what is known about the clay mineralogy on the Hanford Site and the XRD identification from powder mounts. To help confirm this identification, one sample, from 642 ft below the surface, which appears to be entirely clay, was chosen to be analyzed by preparing a clay mount. The clay mount was analyzed after drying in air and then again after exposure to an atmosphere containing ethylene glycol. Figure 3.1 shows that the location of the first diffraction peak in air is ~13 Å, and the location of the same peak in ethylene glycol is ~17 Å. The peak shift confirms that the clay is expanding and matches the properties of a smectite.

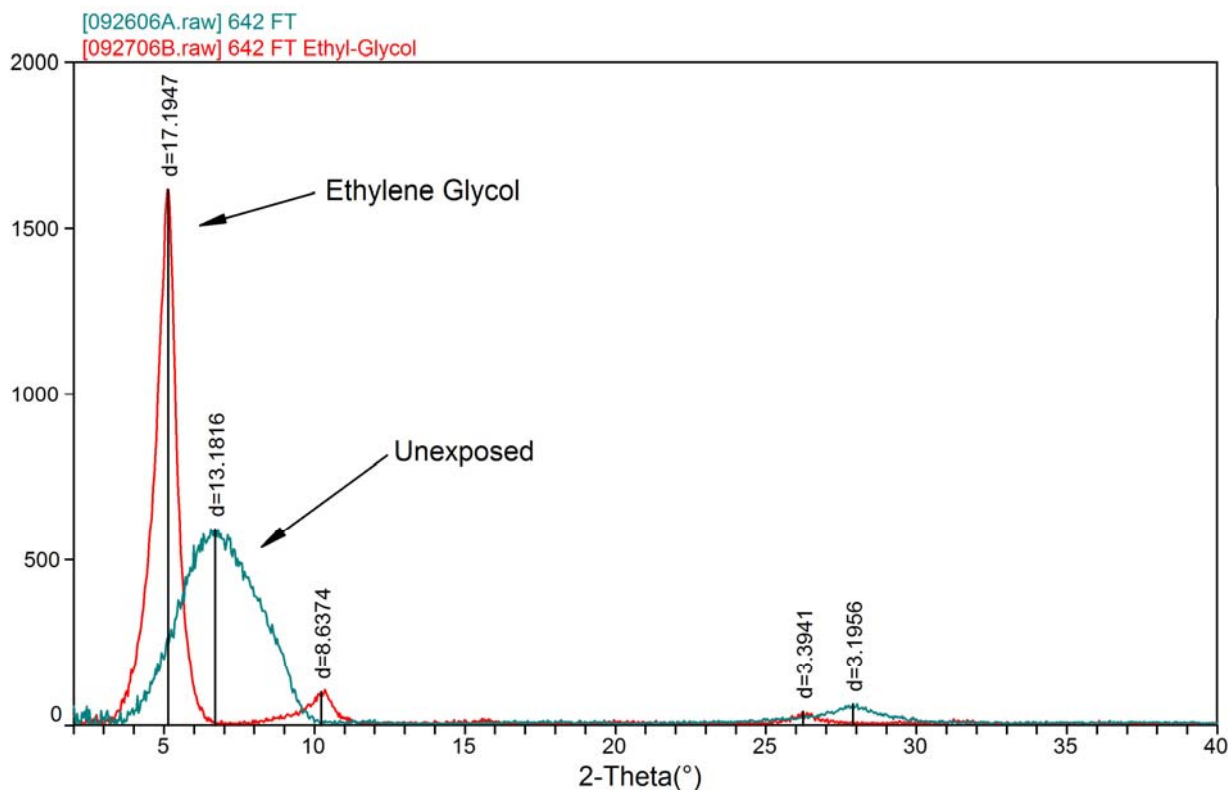


Figure 3.1. Comparing the Clay at 642 ft With and Without Ethylene Glycol Treatment

Plagioclase was the second most abundant mineral identified, present in 49% of the samples measured. It is seen periodically within the entire range of depths measured. Plagioclase was the major phase in 11%, the minor phase in 22%, or a trace phase in 67% of the samples containing plagioclase. Plagioclase was almost exclusively a trace phase when present in the fracture fill samples. The best PDF match for the plagioclase phase was anorthite (41-1486).

Quartz was identified in 24% of the samples at depths ranging from 1219 to 1360 ft. Quartz was the major phase in 56%, the minor phase in 22%, and a trace phase in 22% of the samples containing quartz. The best PDF match was (46-1045).

Pyroxene was identified in 16% of the samples at depths ranging from 631 ft to the maximum depth cored at 1375 ft. Pyroxene was present only as a trace phase. The best PDF match for pyroxene was diopside (60-6805).

Carbonates, siderite and rhodochrosite, were identified in 16% of the samples periodically at depths ranging from 954.5 to 1231.5 ft. Rhodochrosite was identified in only one sample, and it was as a minor phase in combination with siderite. Siderite was the major phase in 67% and once each as a minor and trace phase in samples that contained siderite. The best PDF matches for siderite and rhodochrosite were 63-4344 and 65-3952, respectively.

Zeolite was identified as the major phase in 11% of the samples at three locations of 964, 1020, and 1090.3 ft. Three different zeolites were identified: zeolite P (63-4549), harmotome (60-1661), and clinoptilolite (65-1779).

A few samples contained minerals different than those seen from the many fractures sampled. First is a sample from 519.1 ft, which is mainly opal (crystallite size of $\sim 10\text{-}50 \text{ \AA}$) with trace amounts of anorthite and quartz. Second, is a sample from 561.0 ft, described as chalcedony, which is mainly cristobalite and possibly some tridymite. Third, is a sample from 954.4 ft, described as a sulfide mineral, which clearly contains both pyrite and vaesite. Last, is a sample from 1090.3 ft, described as a black botryoidal mineral, which the very faint XRD pattern in Figure A.24 indicates might be hematite.

Several samples were extremely limited in quantity and once powdered, they were well below the amount required to ideally perform a powder mount. The peak intensities of these samples are very low and in many cases, the patterns only show a single major peak or a few of the major peaks. In these cases, the results are suspect and, if possible, should receive more sample characterization to confirm these results.

In some of the scans shown in the appendix, there are peaks that are labeled as tungsten. These peaks are small and are only seen when the sample contains high concentrations of quartz or siderite, which provides intense reflections. The X-ray tube used for this work has a copper target; however, due to the old age of the tube, enough tungsten has been deposited onto the copper target to cause the tube to also emit a very small amount of tungsten X-rays.

There are limitations associated with XRD that should be considered. Identifying phases by XRD is based upon matching up the measured diffraction patterns for an unknown sample to indexed diffraction patterns in the databases. The XRD pattern is a function of the structural characteristics of the mineral(s). The chemical composition of the mineral influences the structural characteristics. However, the

technique does not directly measure chemical composition. Also, in almost all of the samples, multiple phases are present, complicating the identification of the individual phases. For these reasons, the results given in Table 2.1 are more generalized than those given in the XRD figures shown in Appendix A. To confidently identify the phases present in this sample set (e.g., the exact feldspar or clay mineral), the chemical compositions also should be measured at a minimum.

4.0 References

Moore DM, and RC Reynolds, Jr. 1989. *X-Ray Diffraction and the Identification and Analysis of Clay Minerals*. Oxford University Press, Oxford, NY.

Pacific Northwest National Laboratory. 2006. *Sampling and Analysis Plan—Waste Treatment Plant Seismic Boreholes Project*. PNNL-15848 Rev. 2, Pacific Northwest National Laboratory, Richland, WA.

Appendix A

XRD Patterns Showing Mineral Identification

Appendix A: XRD Patterns Showing Mineral Identification

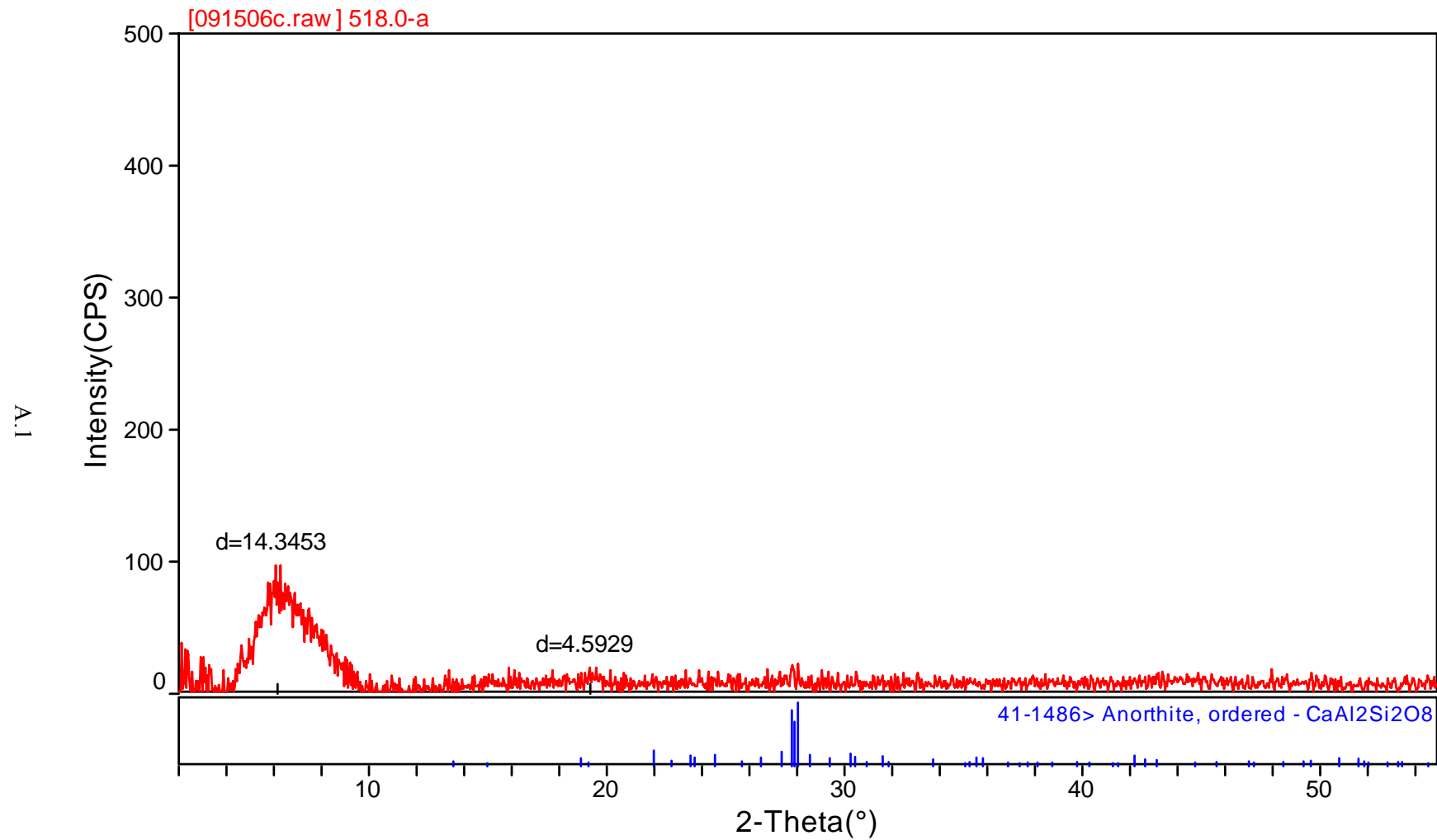


Figure A.1. XRD Pattern for Sample 518-A

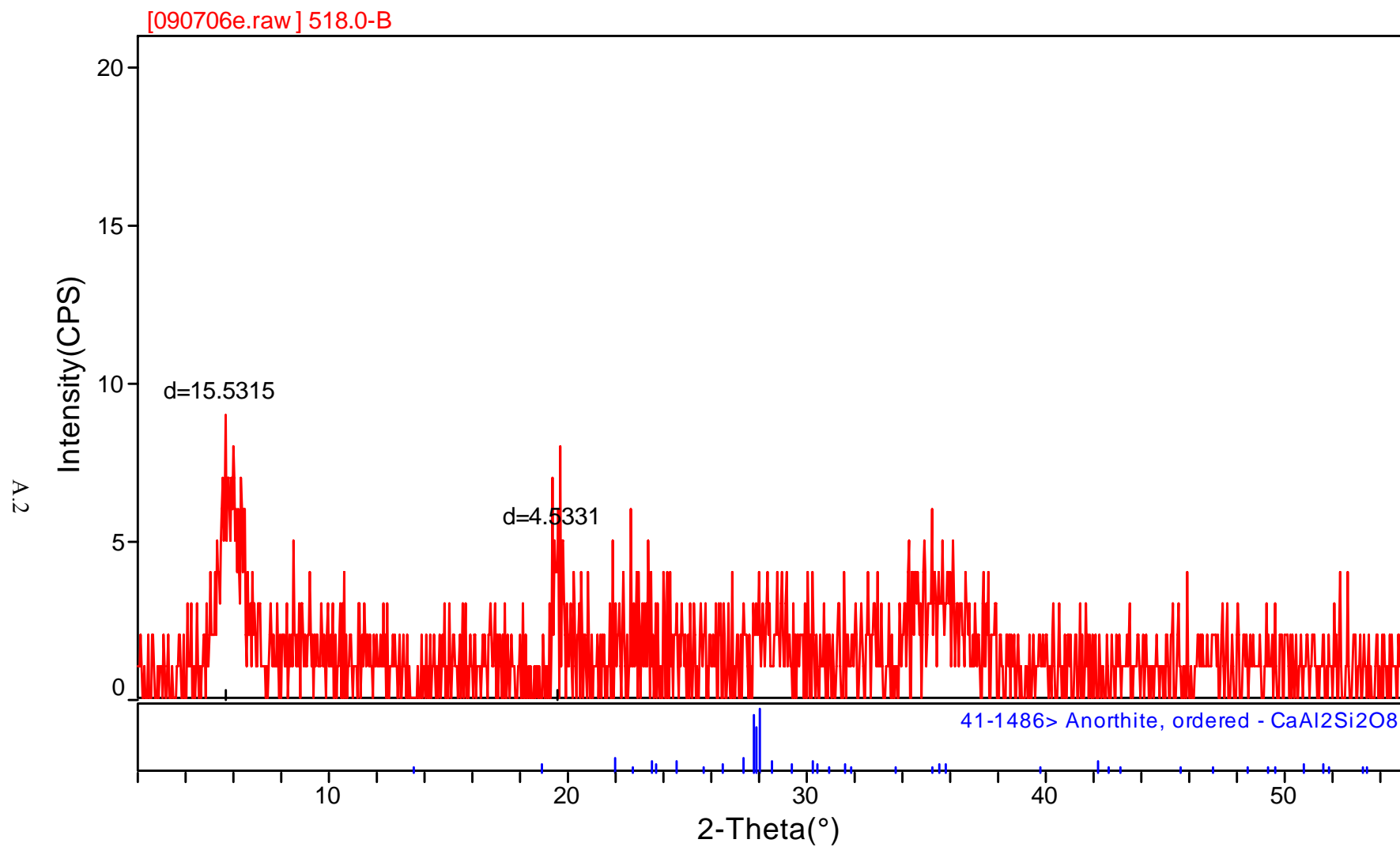


Figure A.2. XRD Pattern for Sample 518-B

A.3

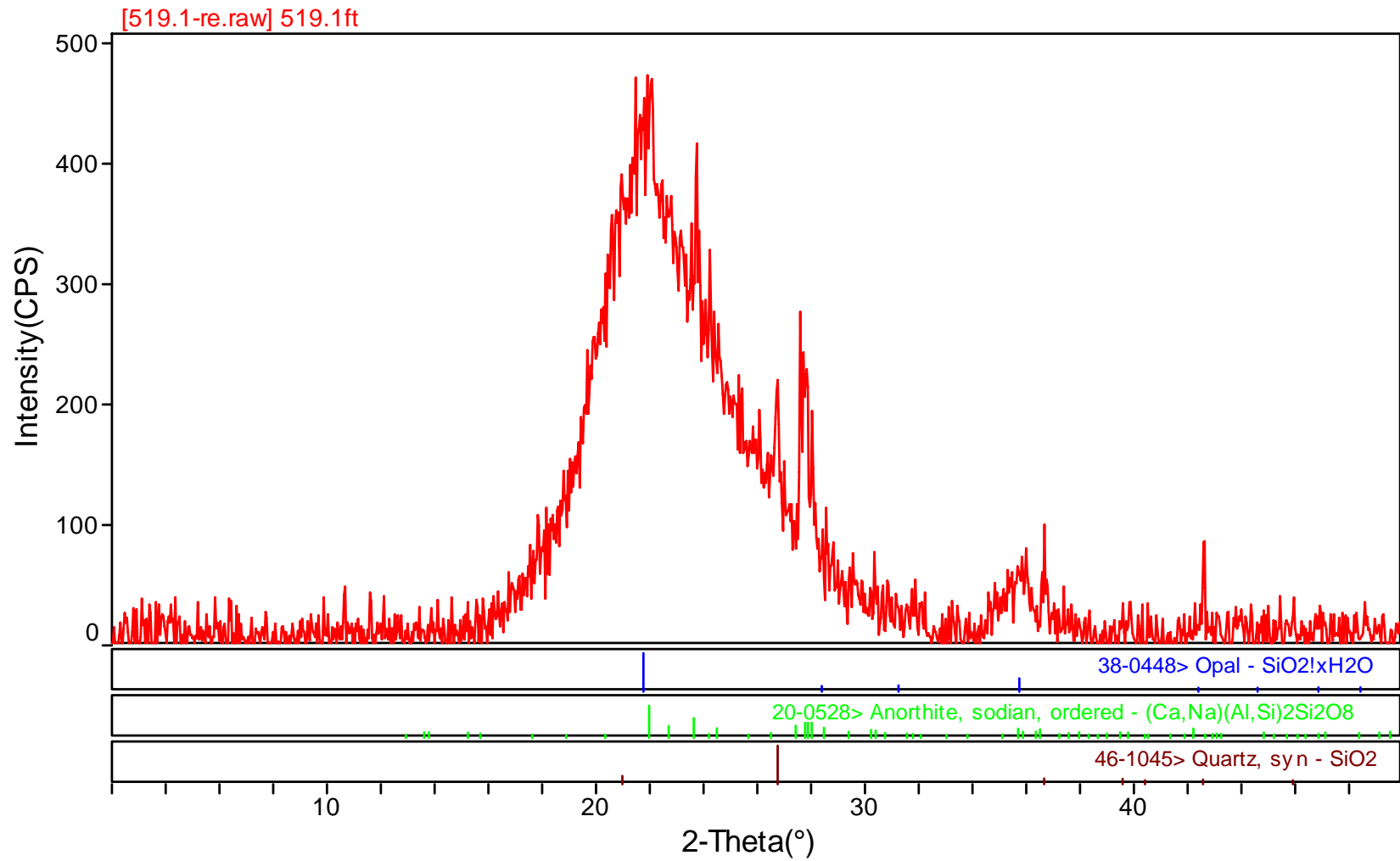


Figure A.3. XRD Pattern for Sample 519.1

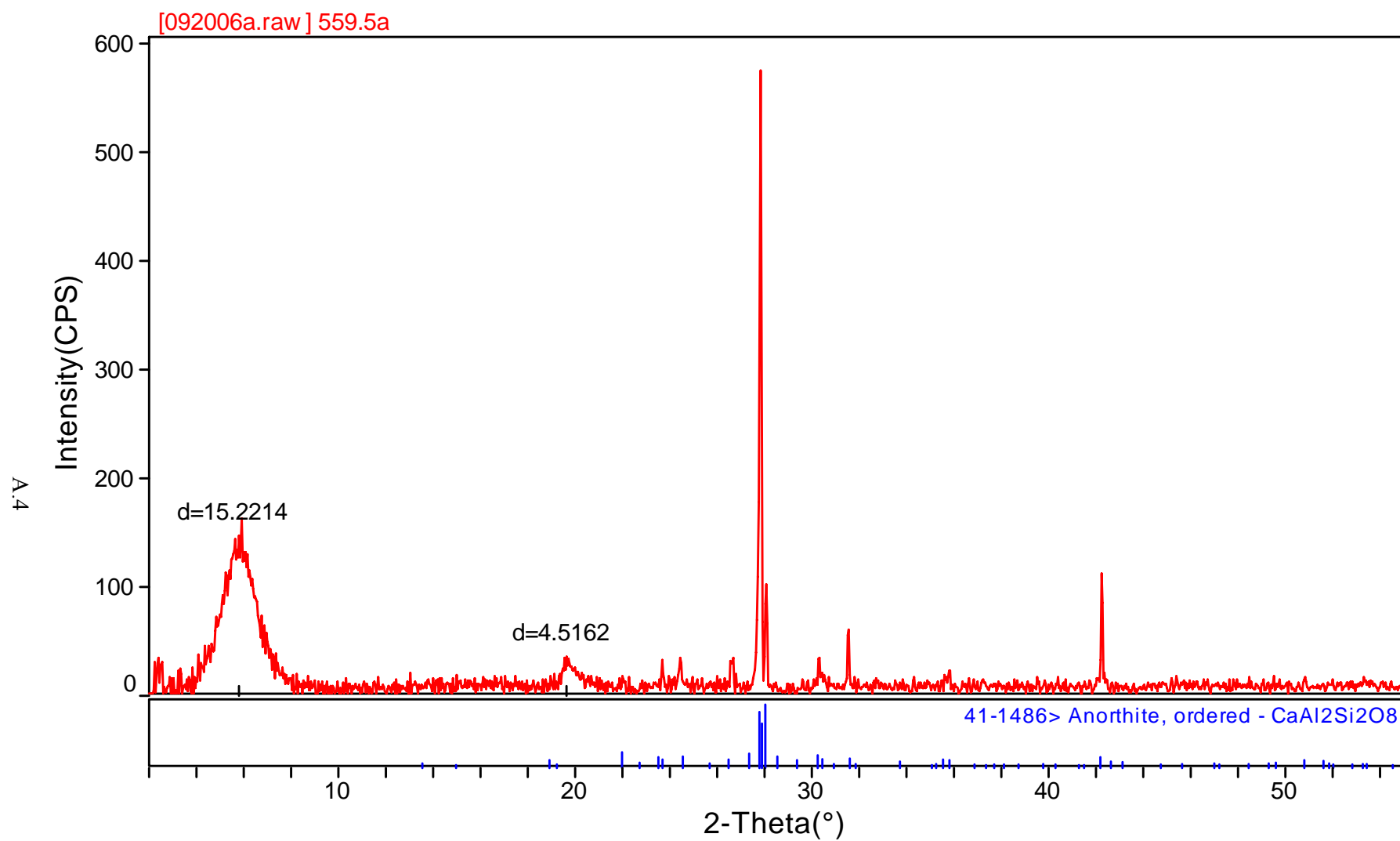


Figure A.4. XRD Pattern for Sample 559.5-A

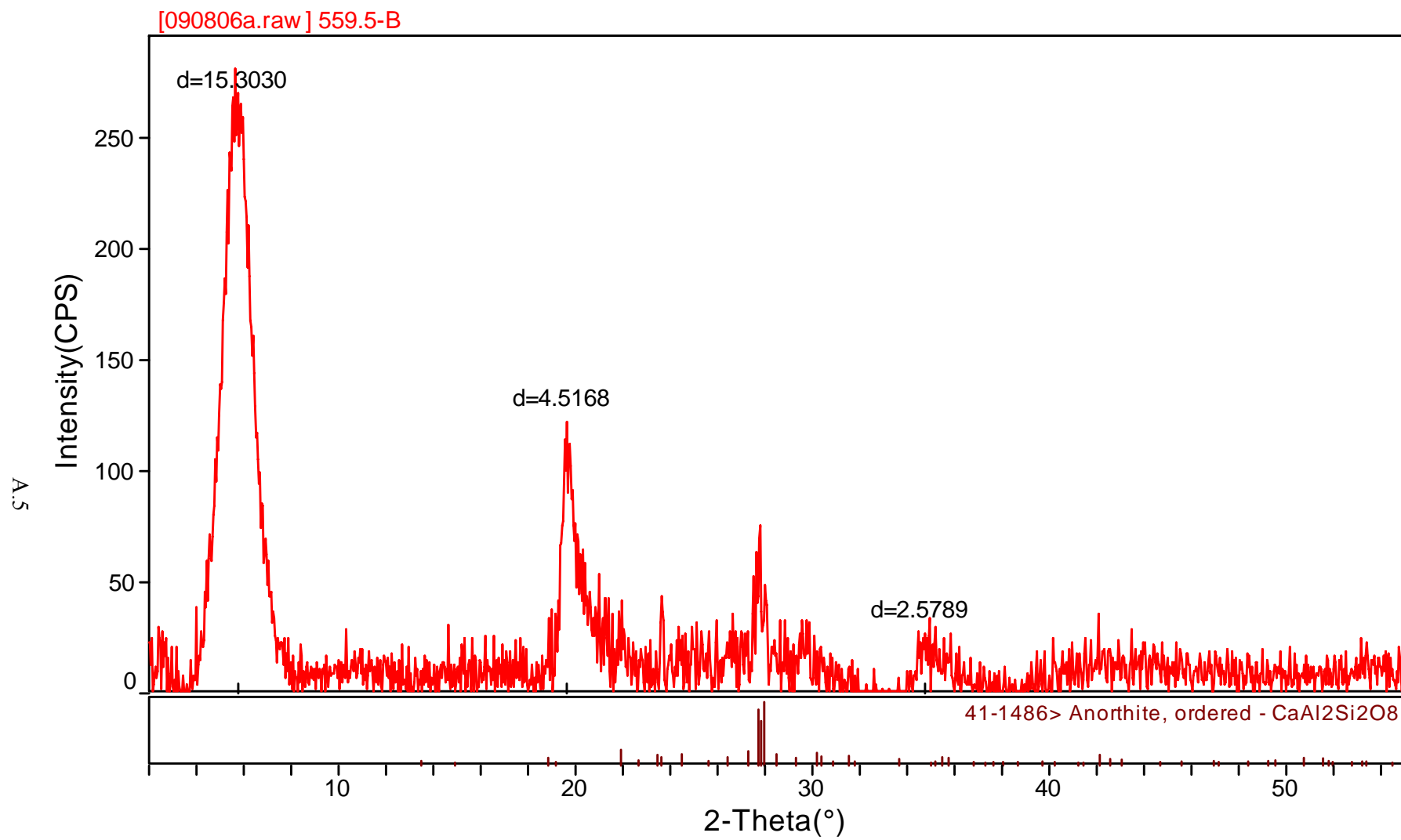


Figure A.5. XRD Pattern for Sample 559.5-B

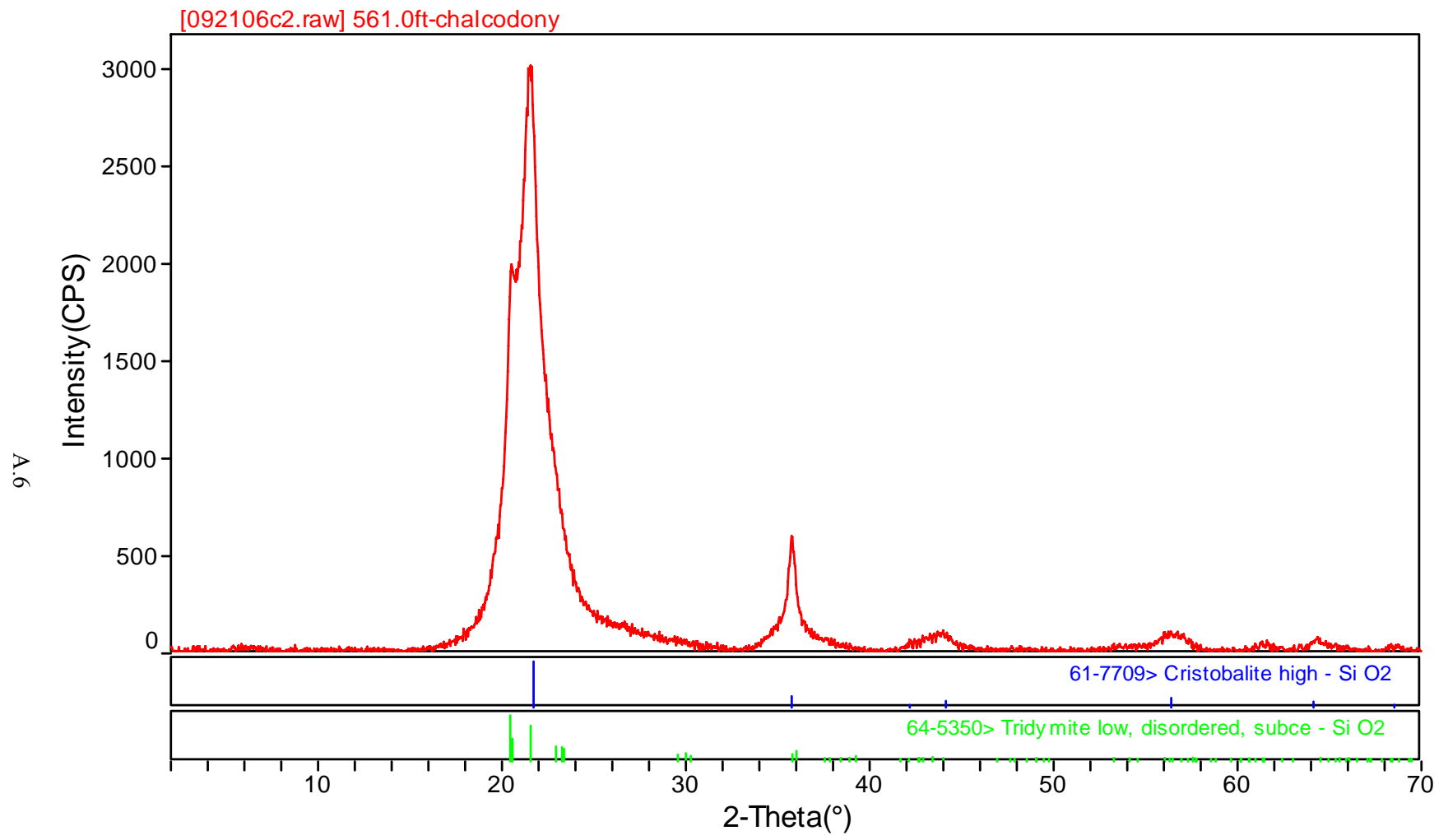


Figure A.6. XRD Pattern for Sample 561.0

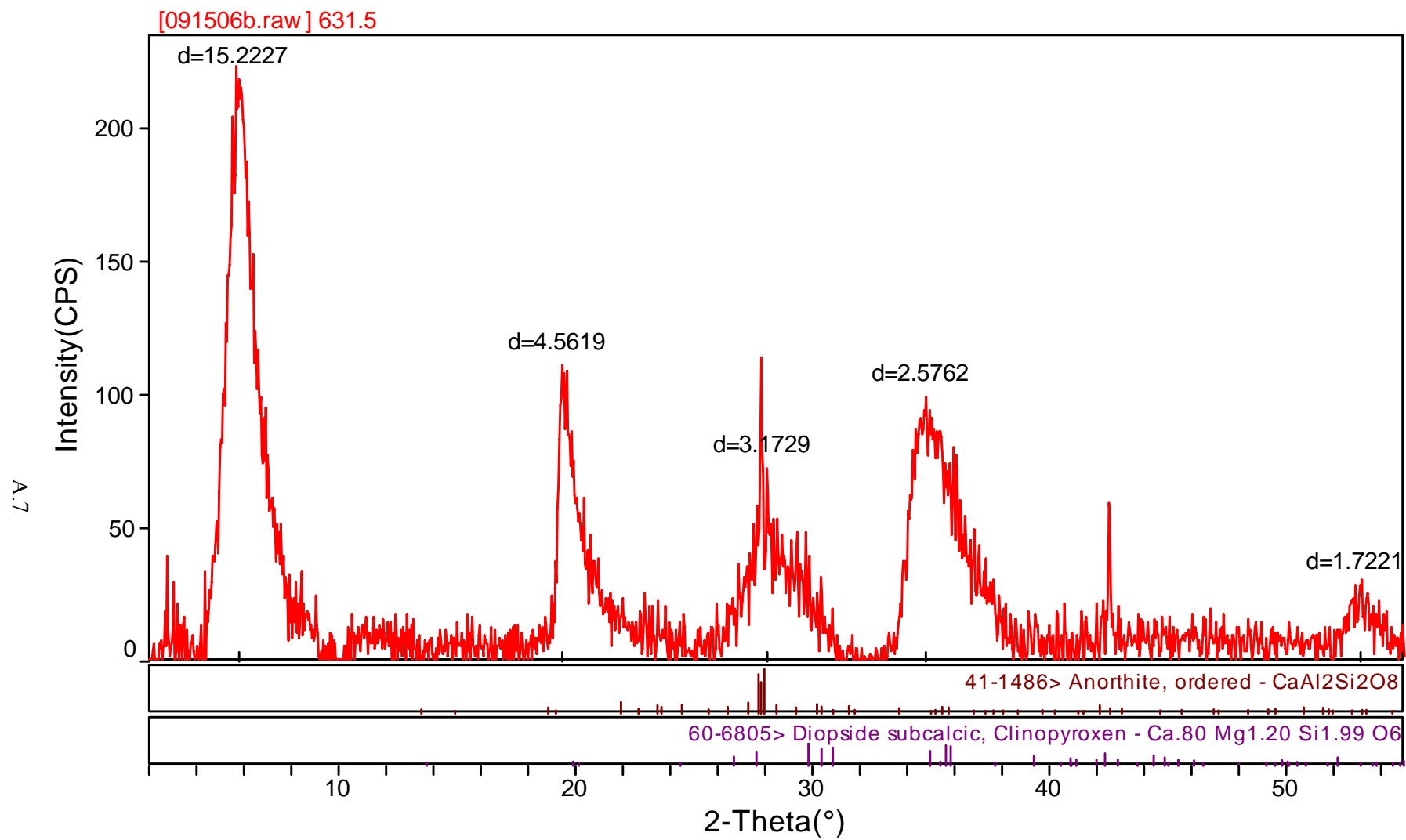


Figure A.7. XRD Pattern for Sample 631.5

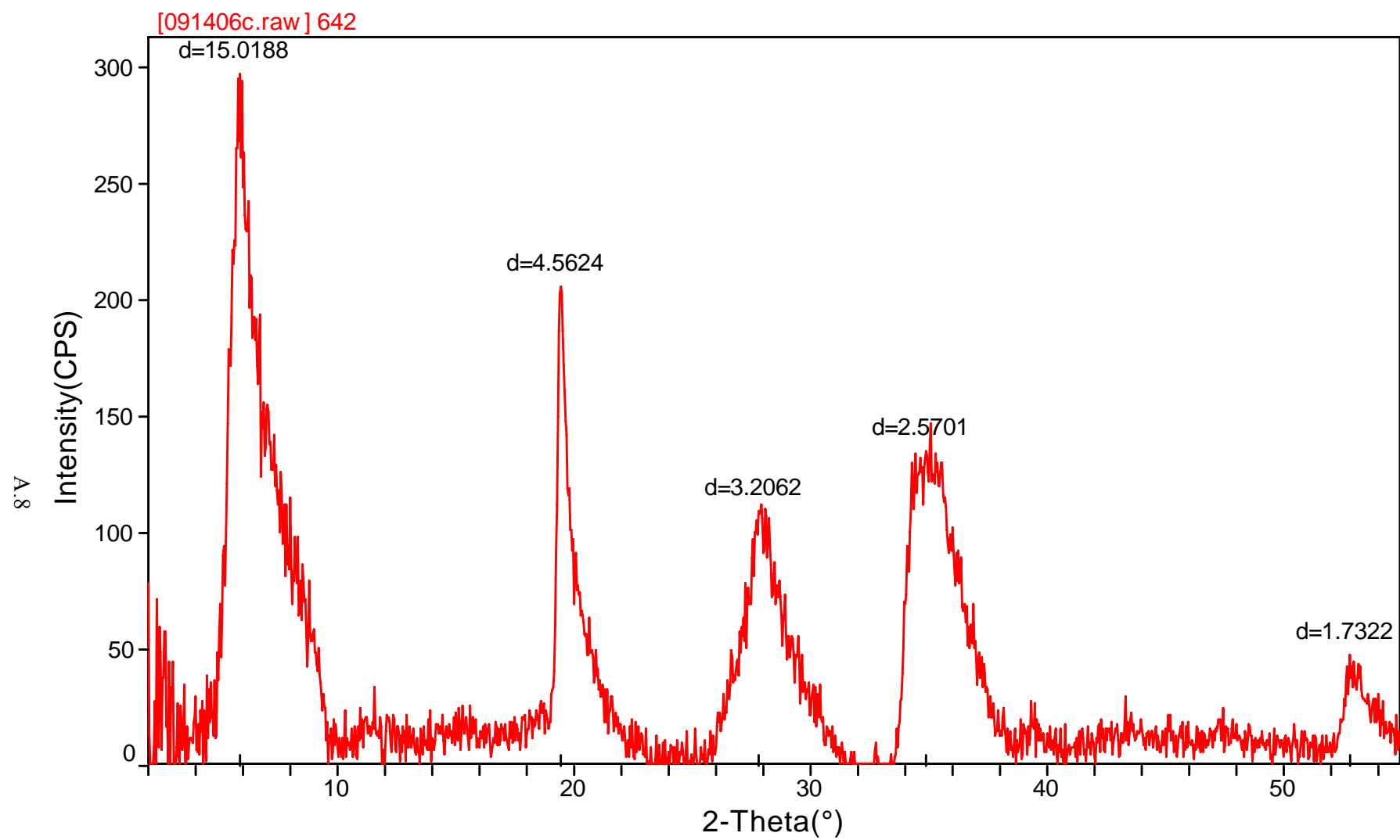


Figure A.8. XRD Pattern for Sample 642

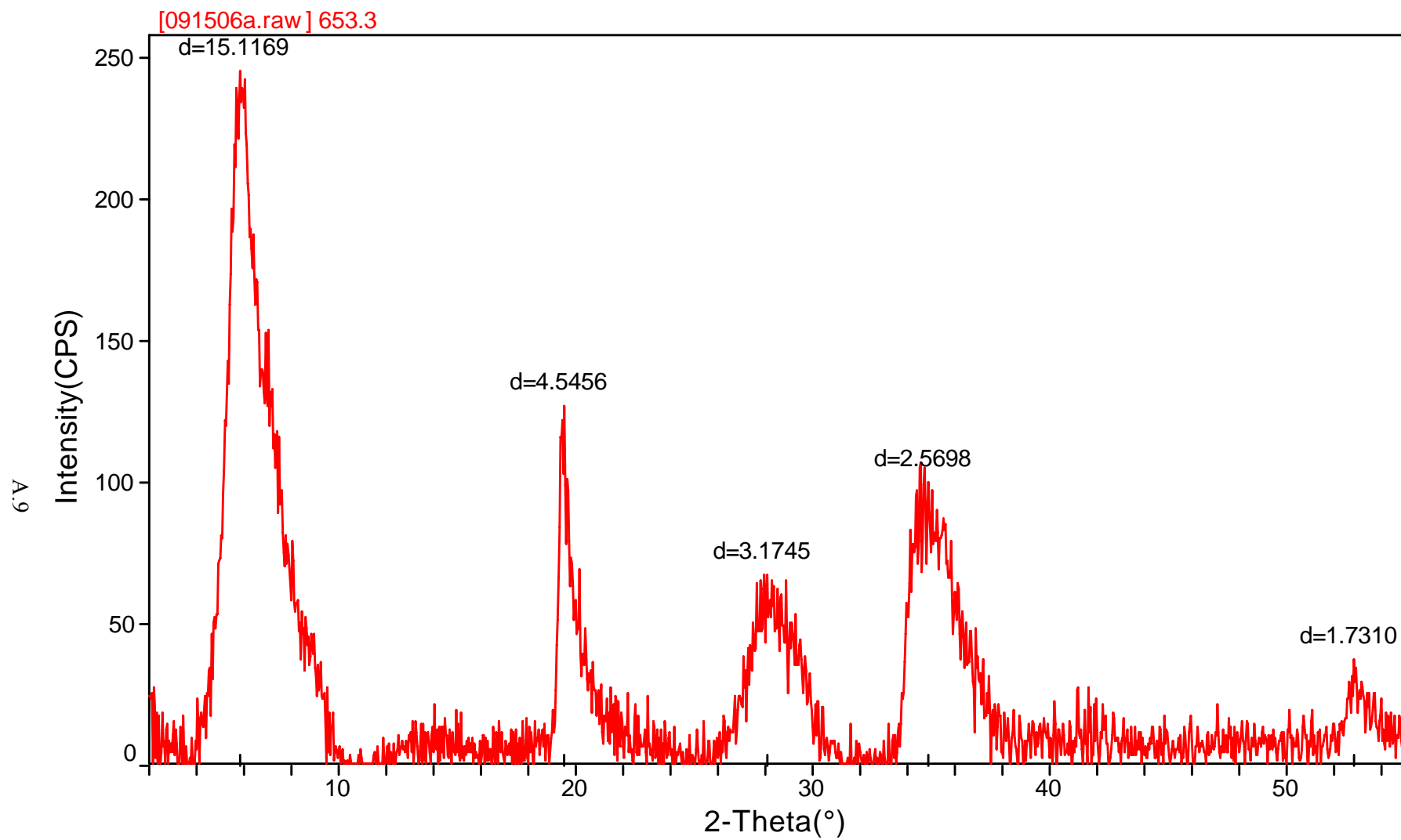


Figure A.9. XRD Pattern for Sample 653.3

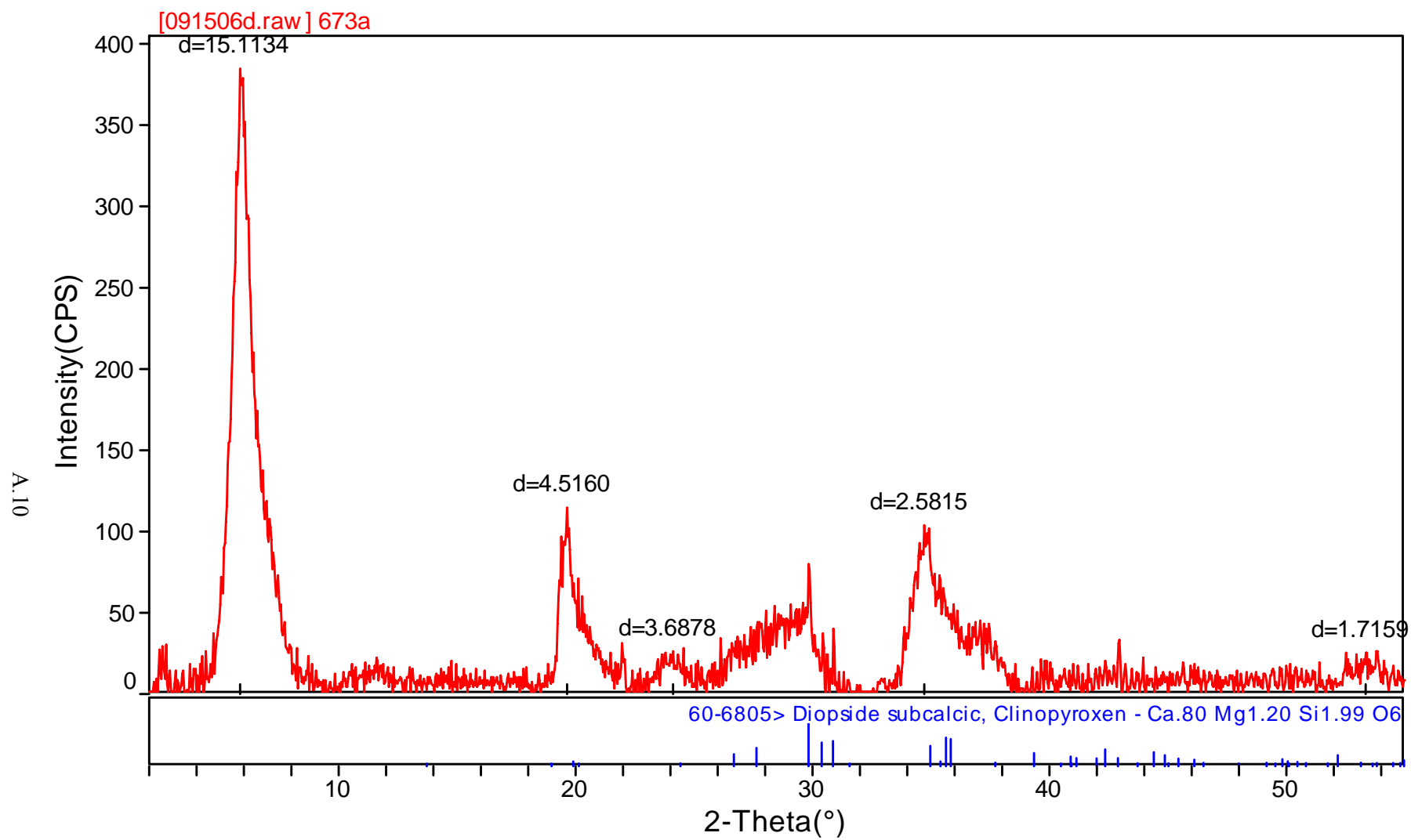


Figure A.10. XRD Pattern for Sample 673-A

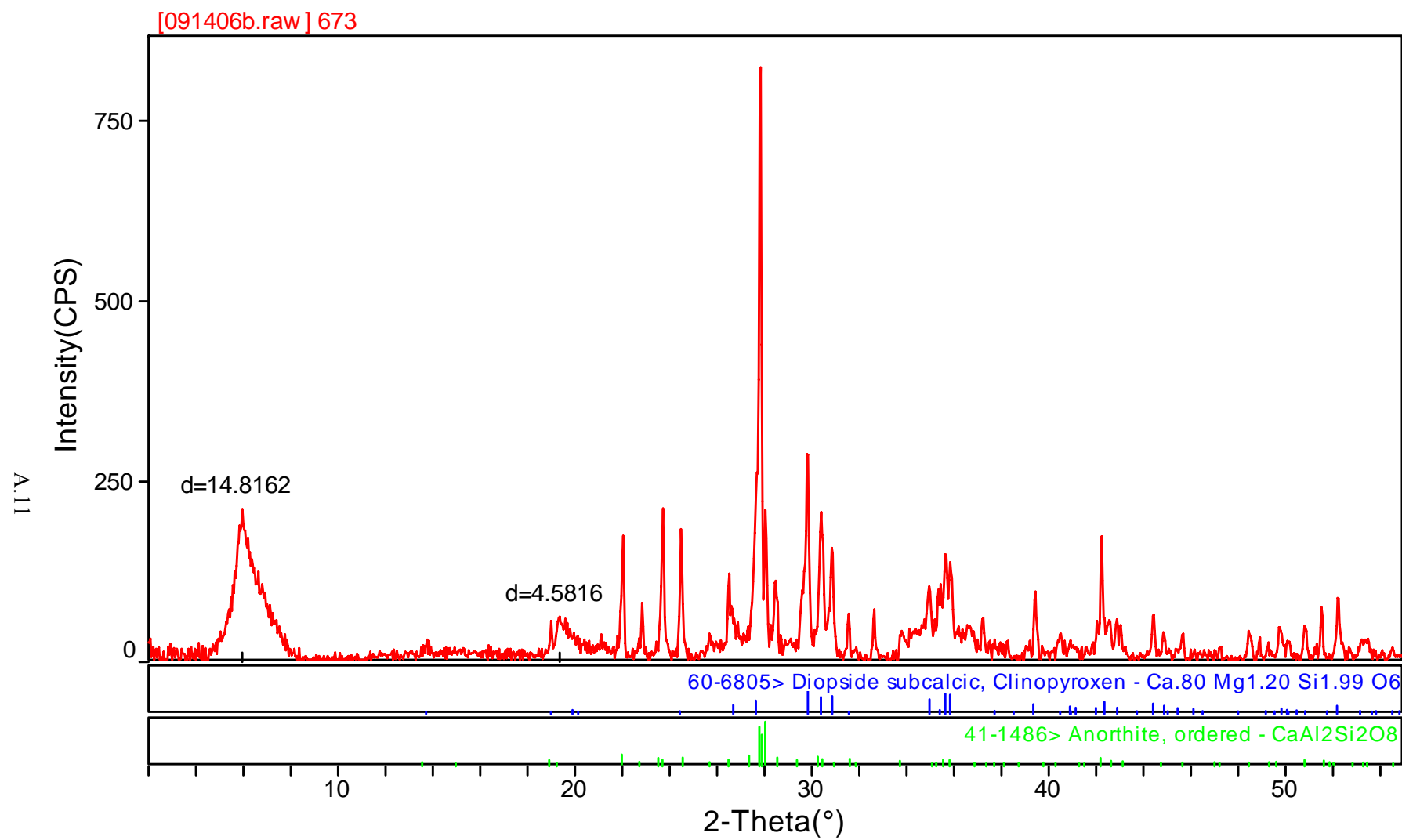


Figure A.11. XRD Pattern for Sample 673-B

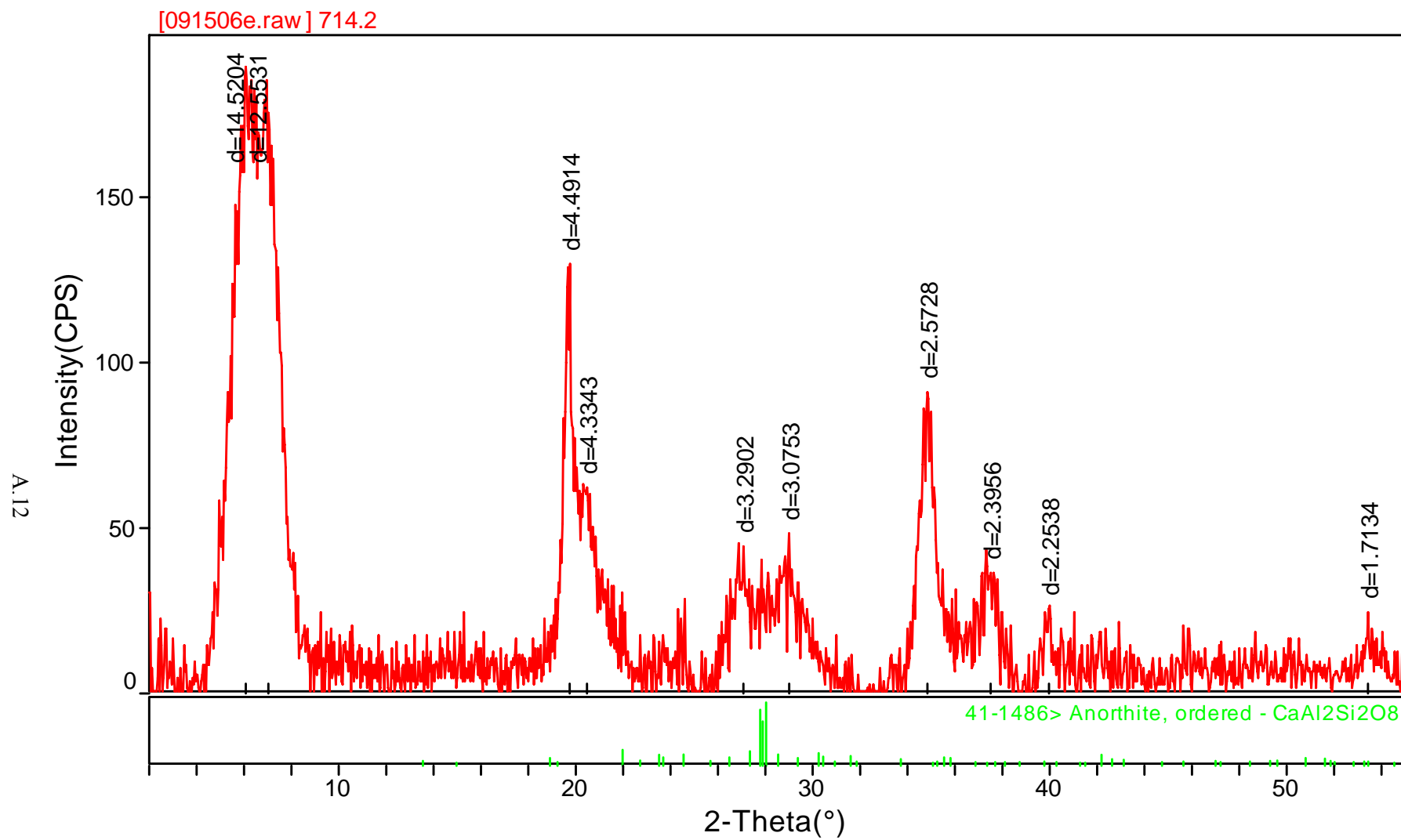


Figure A.12. XRD Pattern for Sample 714.2

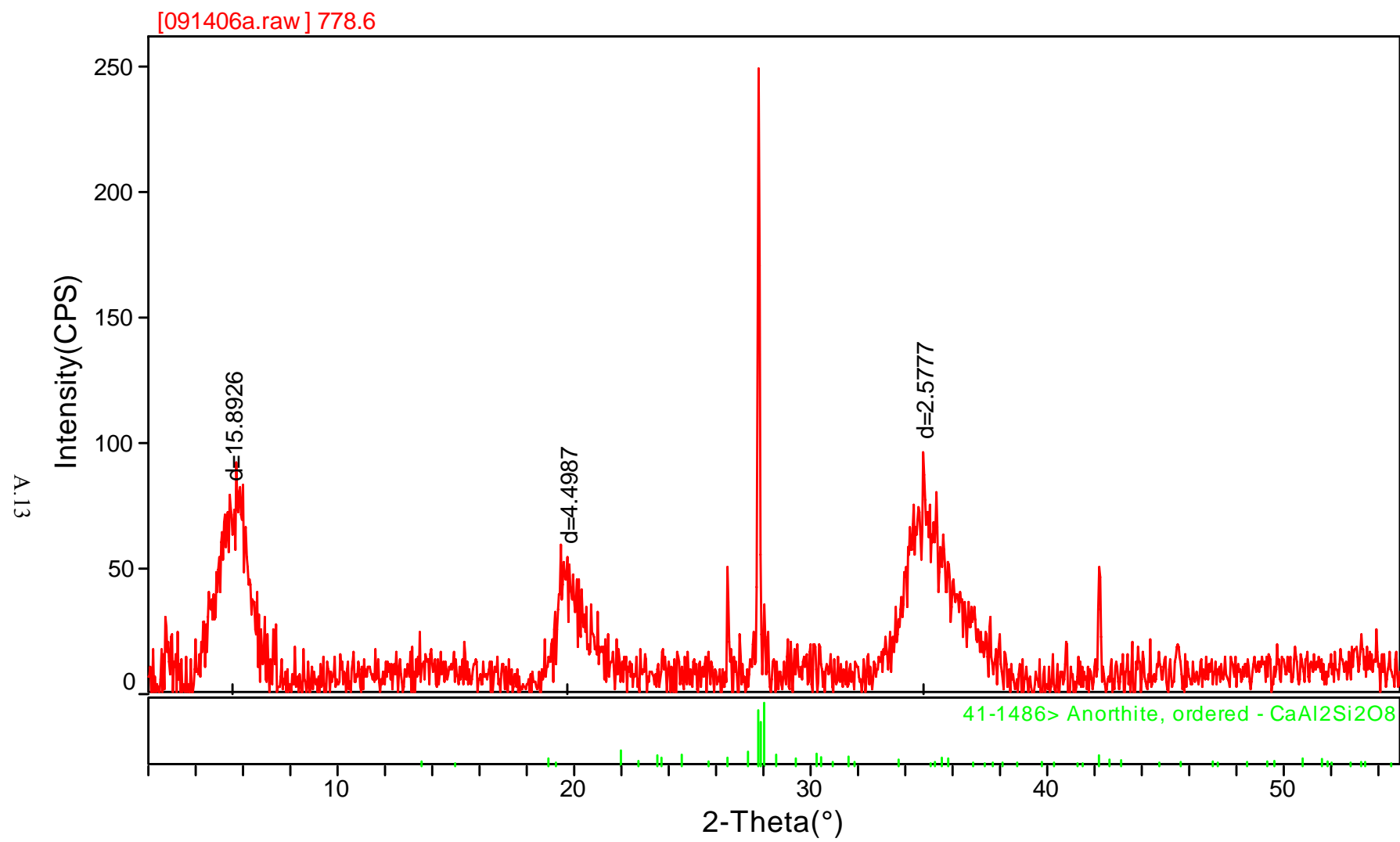


Figure A.13. XRD Pattern for Sample 778.6

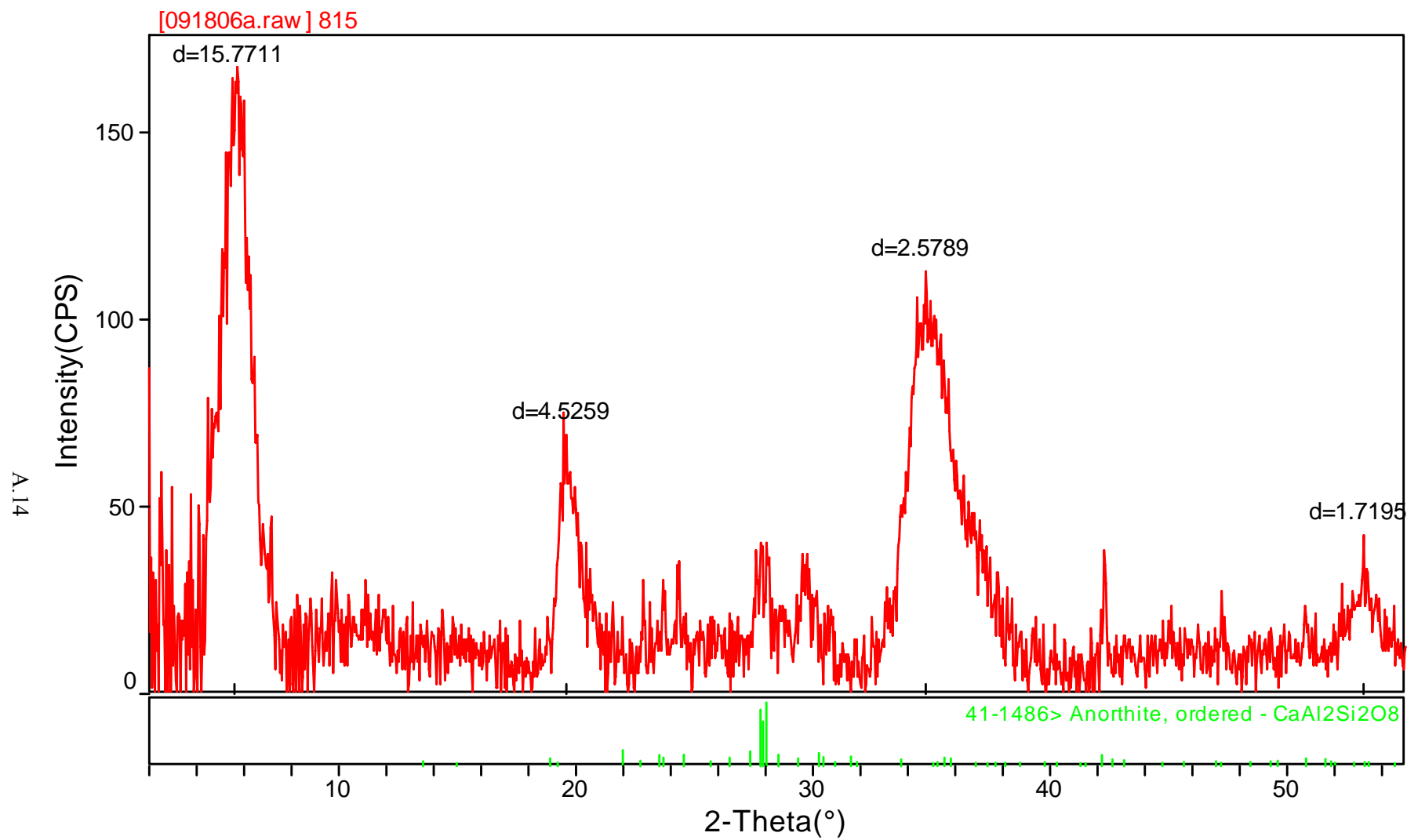


Figure A.14. XRD Pattern for Sample 815

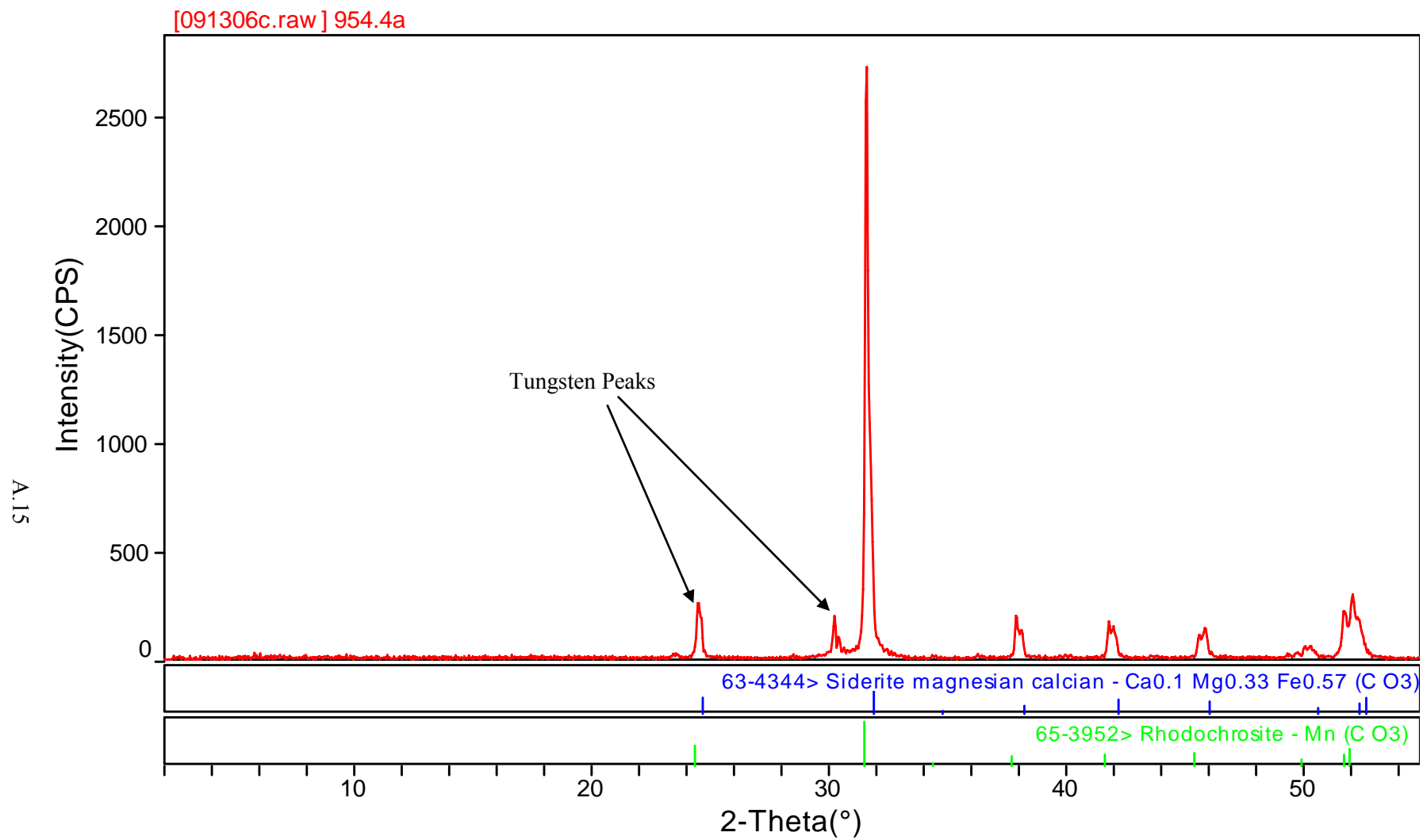


Figure A.15. XRD Pattern for Sample 954.4-A

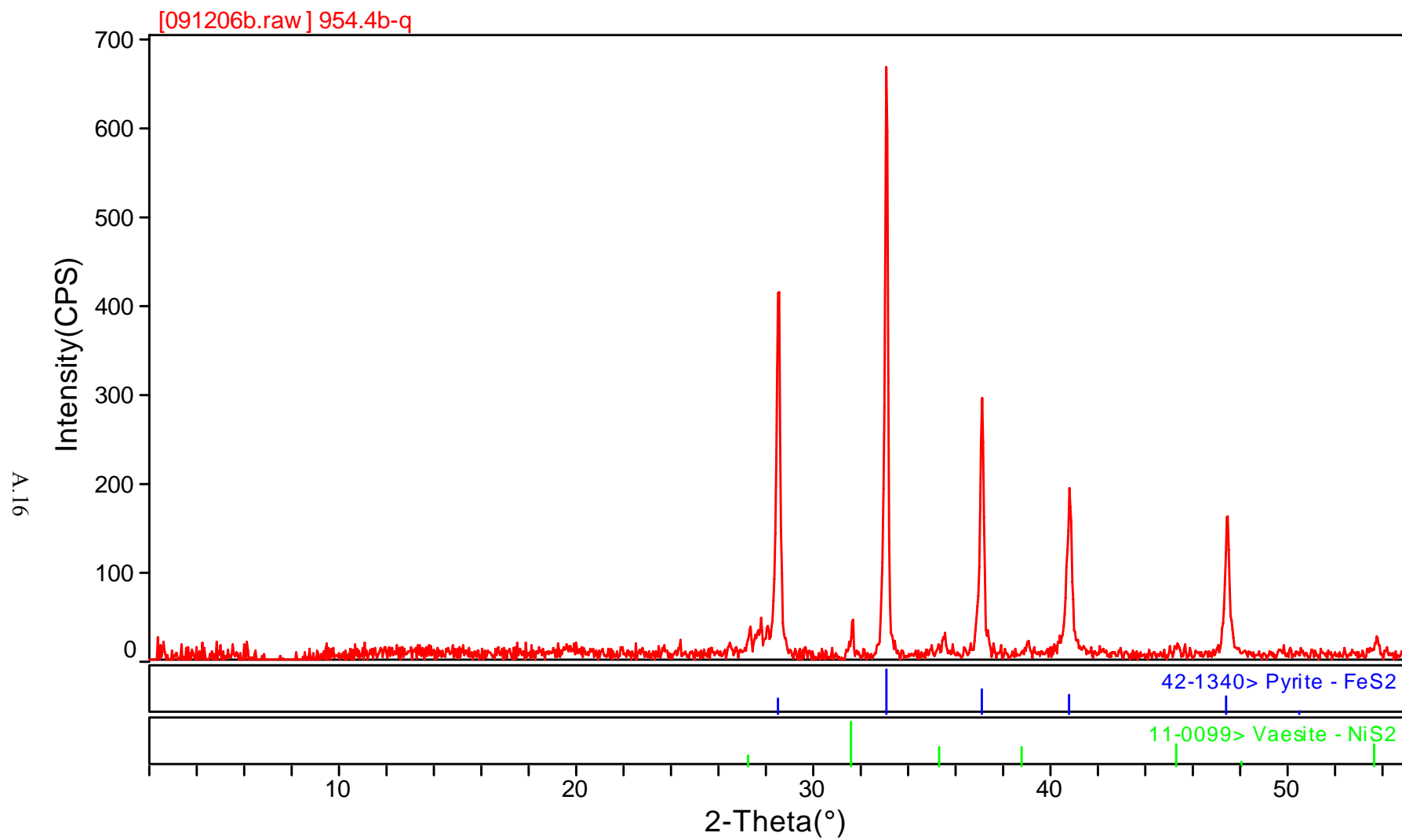


Figure A.16. XRD Pattern for Sample 954.4-B

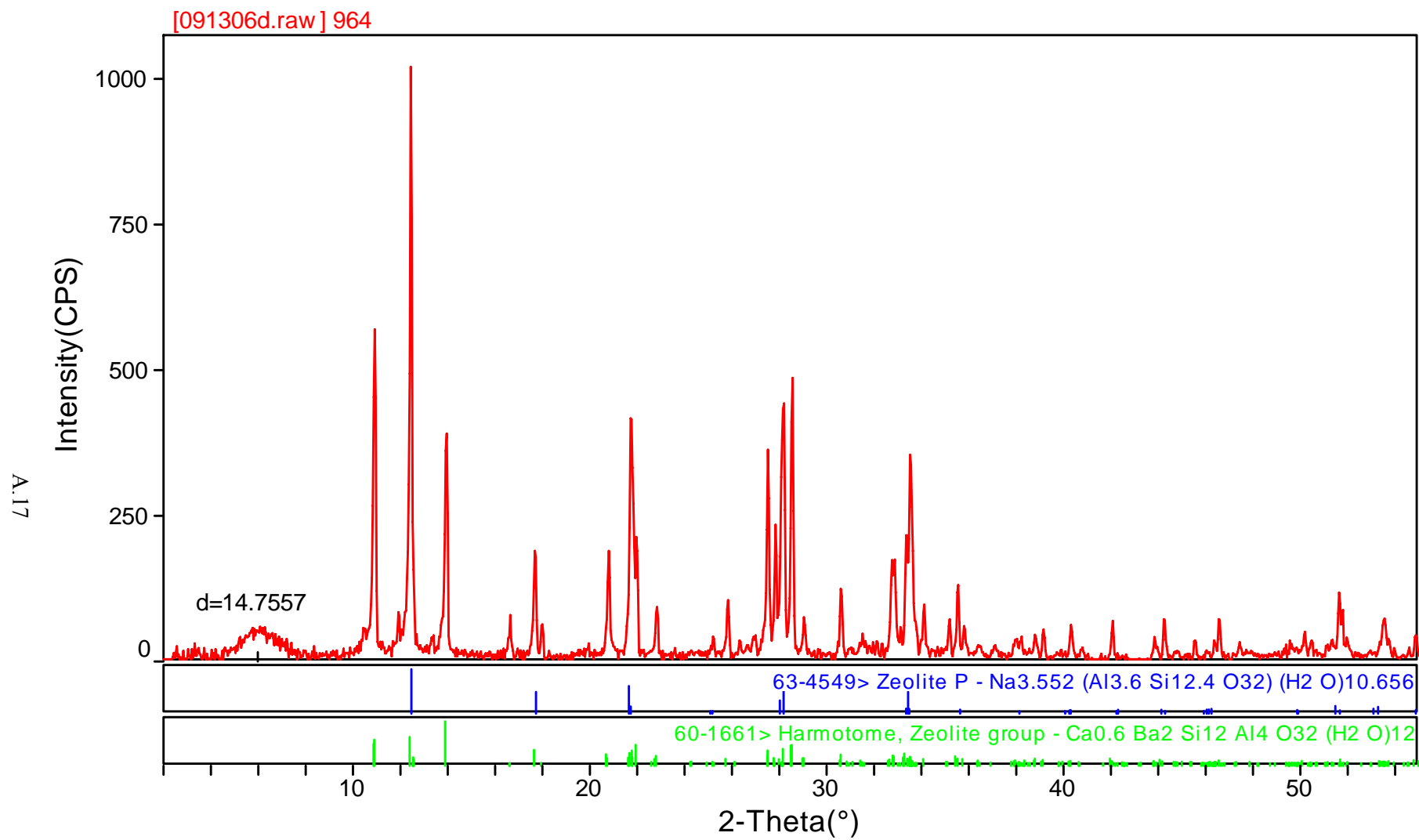


Figure A.17. XRD Pattern for Sample 964

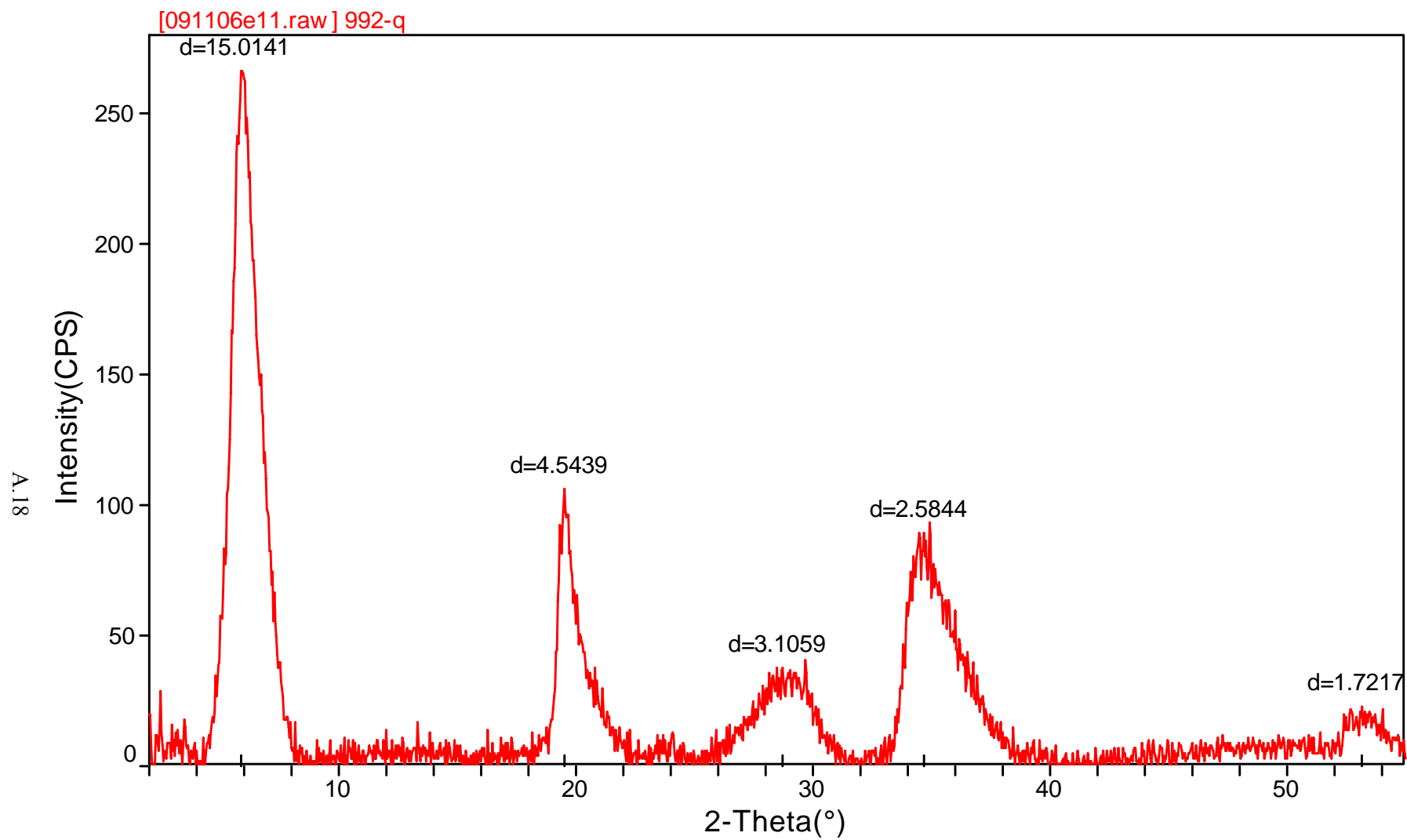


Figure A.18. XRD Pattern for Sample 992

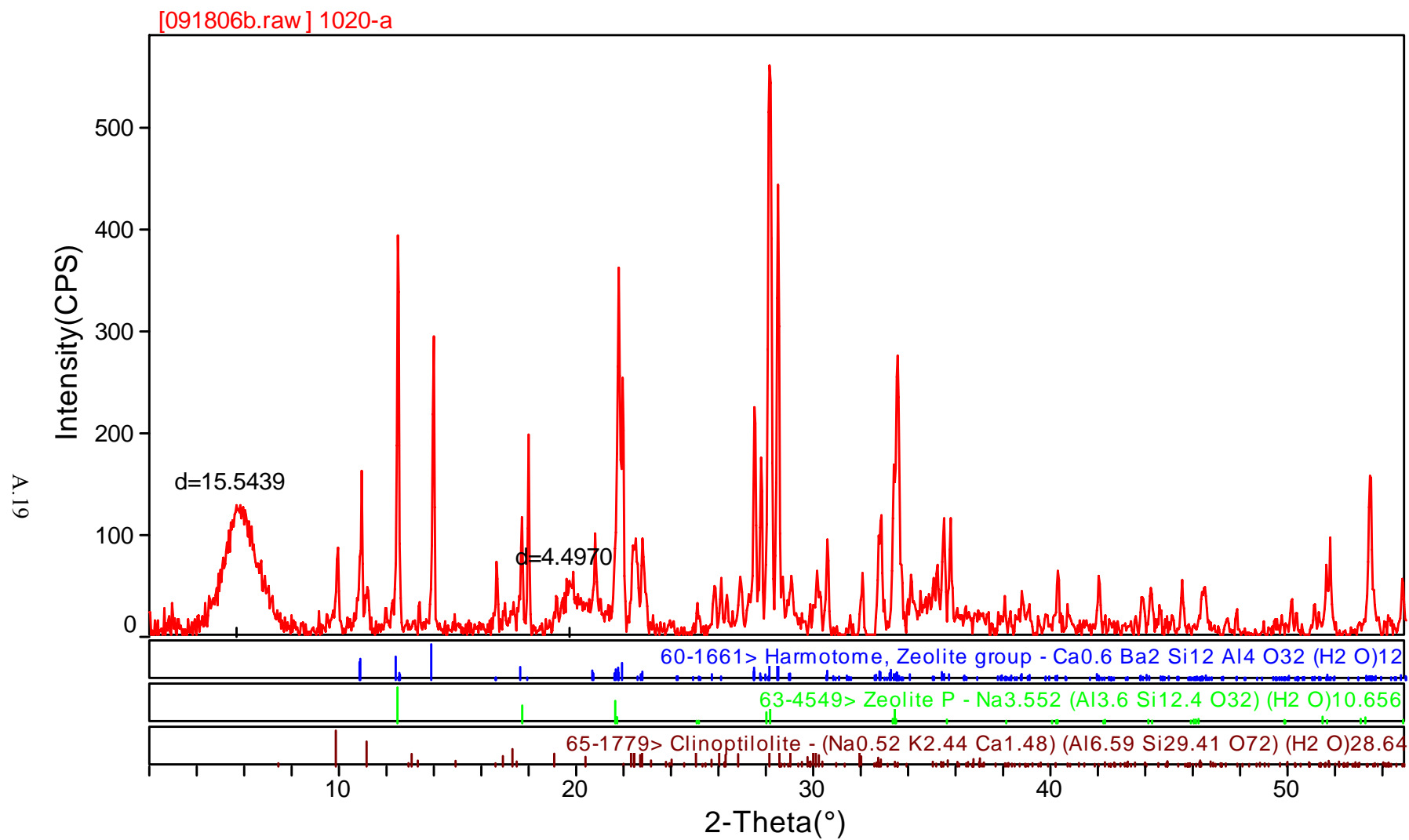


Figure A.19. XRD Pattern for Sample 1020-A

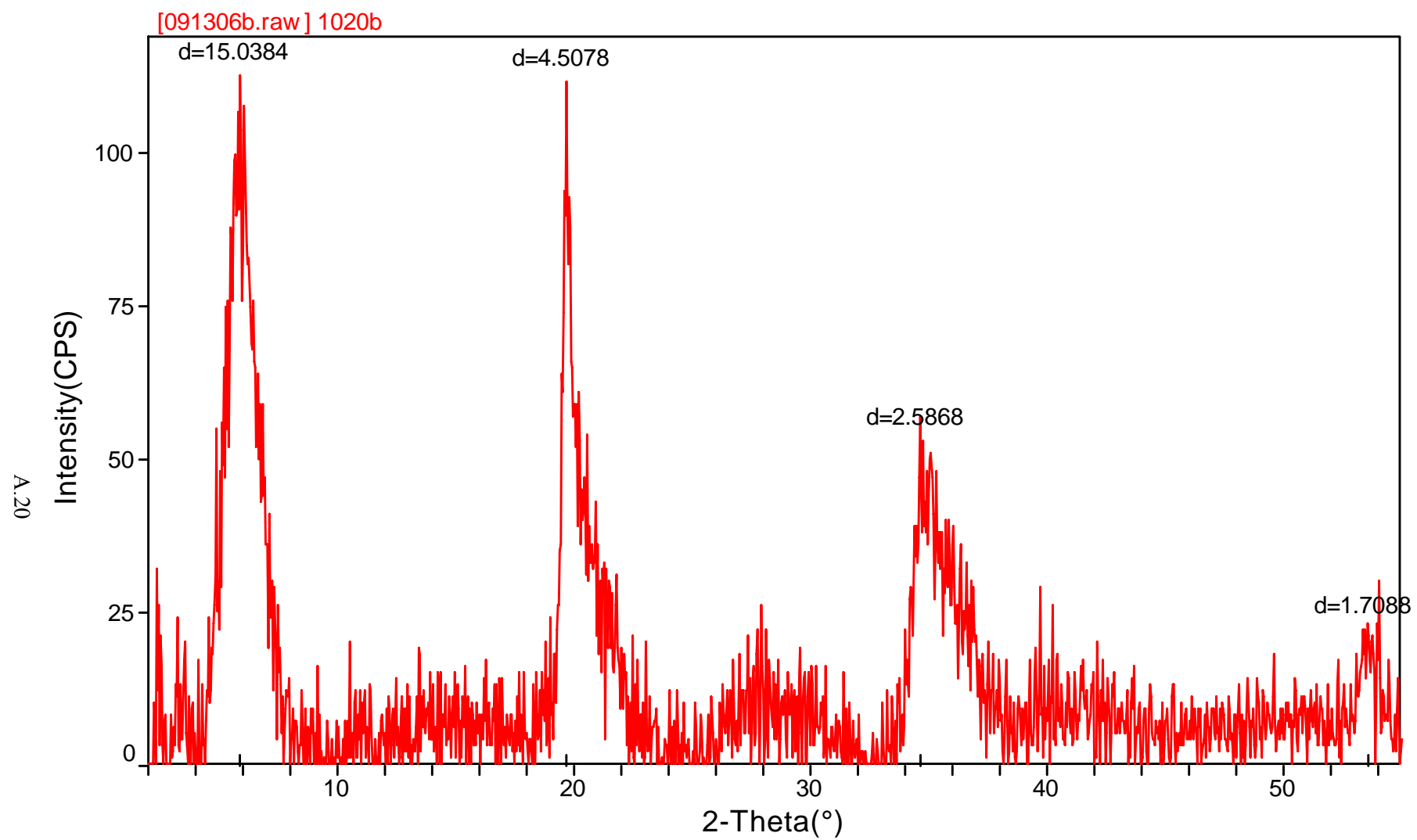


Figure A.20. XRD Pattern for Sample 1020-B

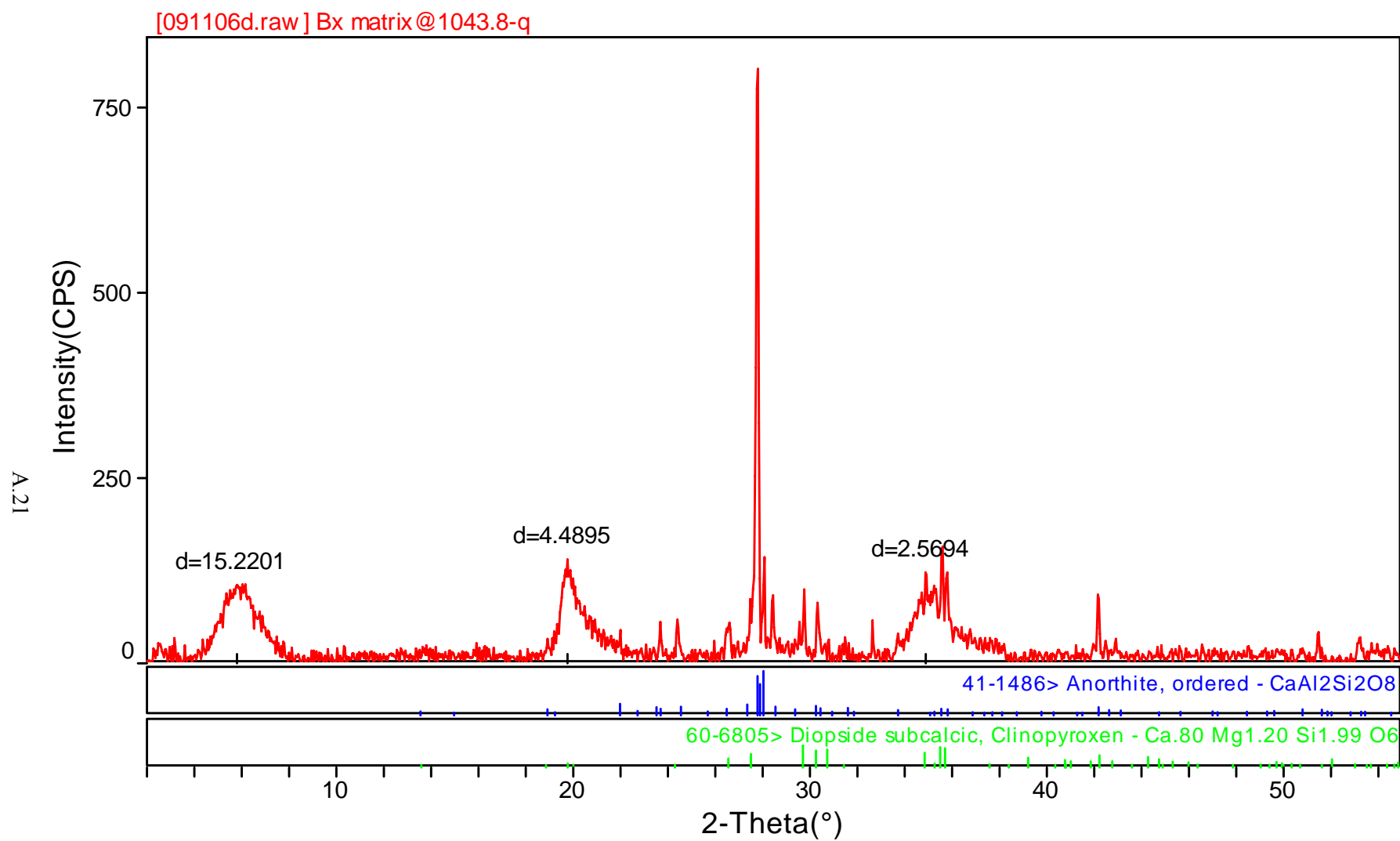


Figure A.21. XRD Pattern for Sample 1043.8

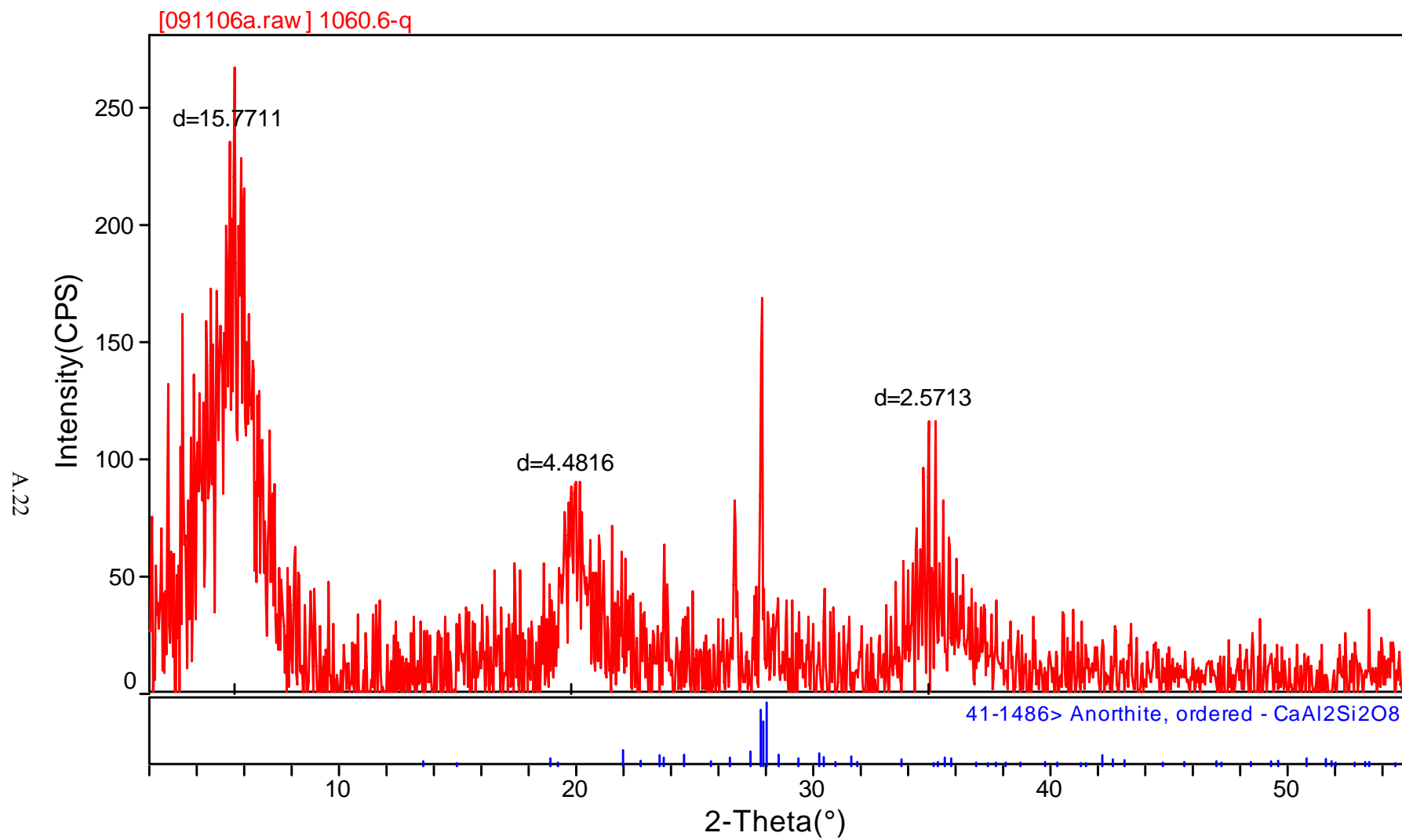


Figure A.22. XRD Pattern for Sample 1060.6

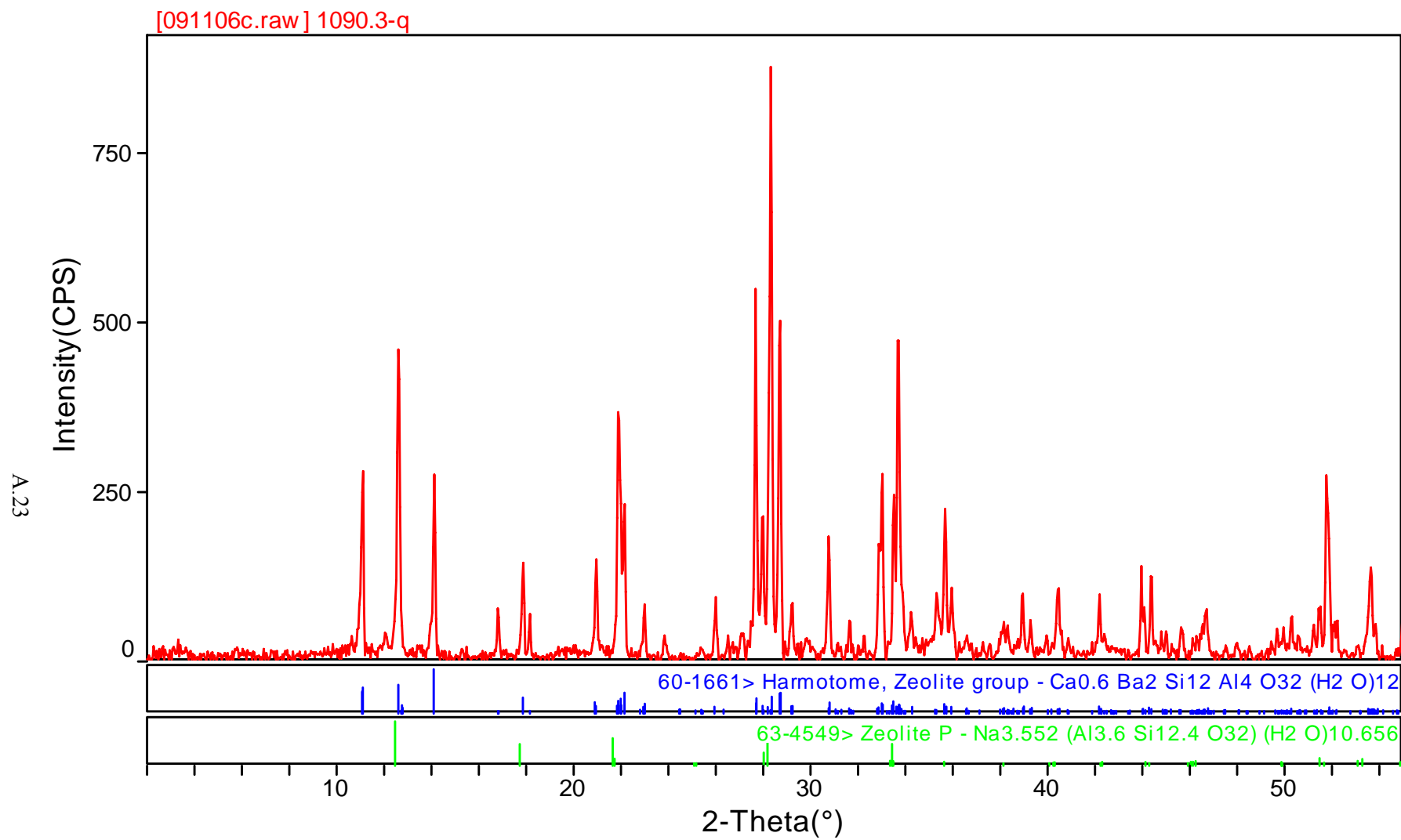


Figure A.23. XRD Pattern for Sample 1090.3

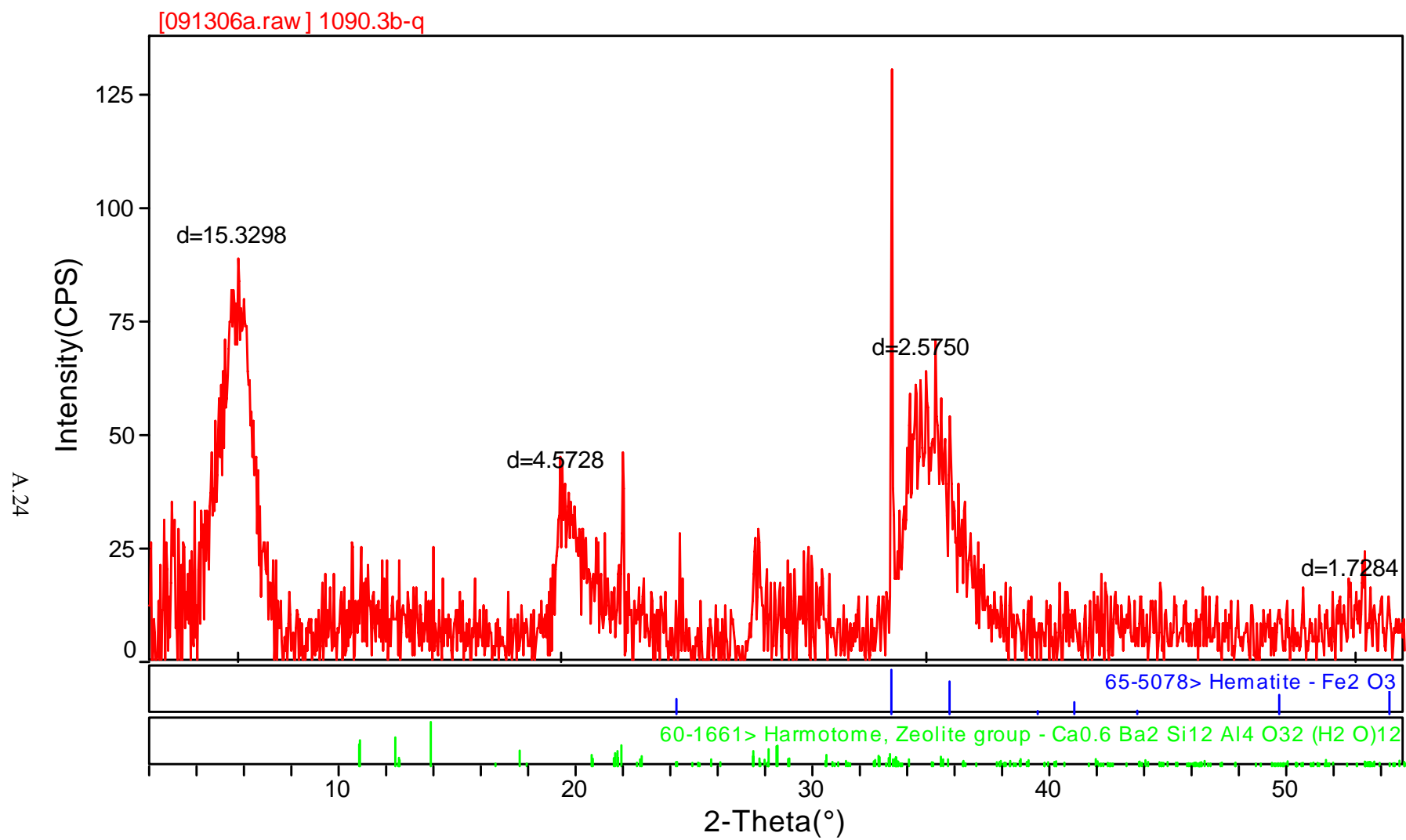


Figure A.24. XRD Pattern for Sample 1090.3-B

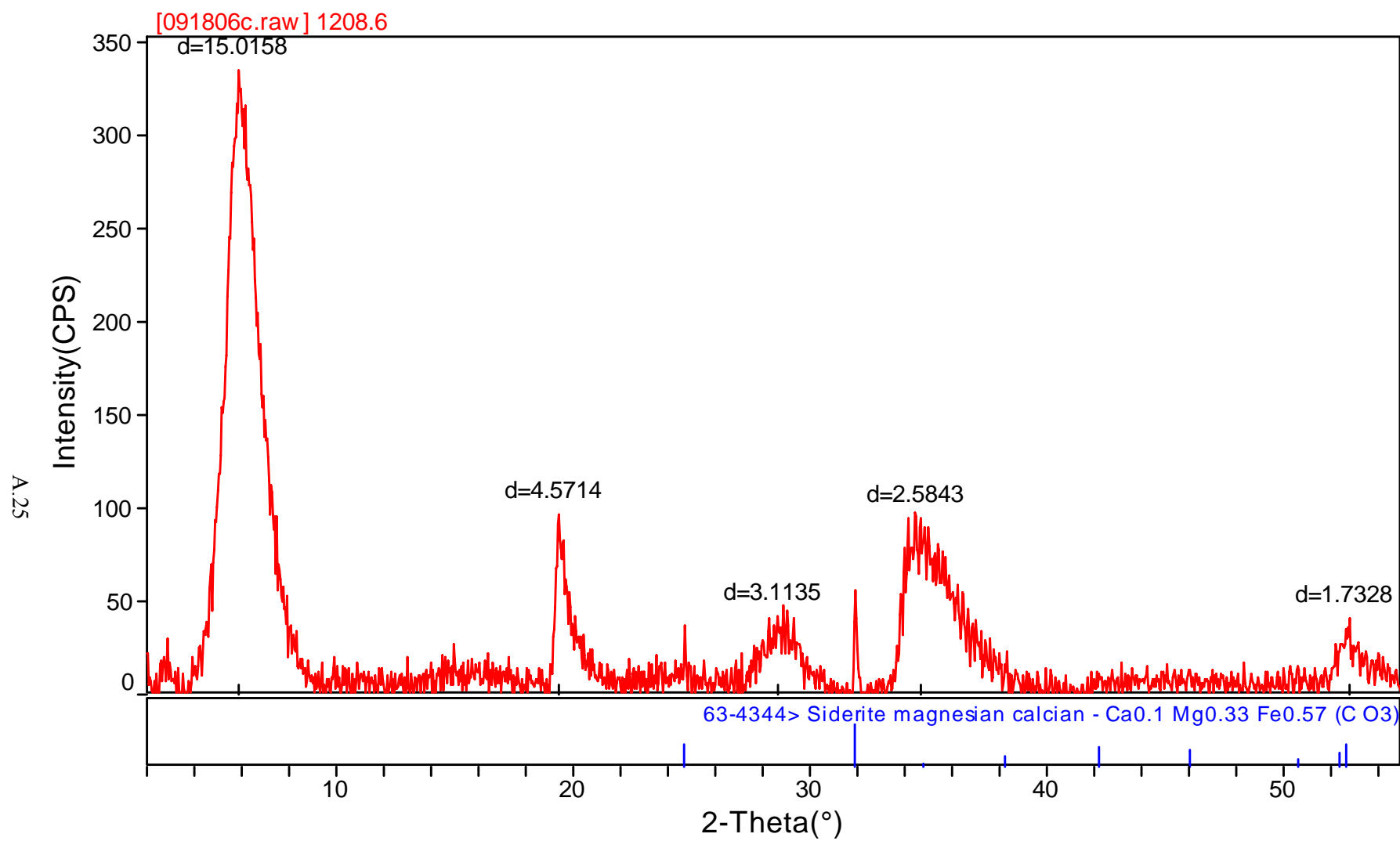


Figure A.25. XRD Pattern for Sample 1208.6

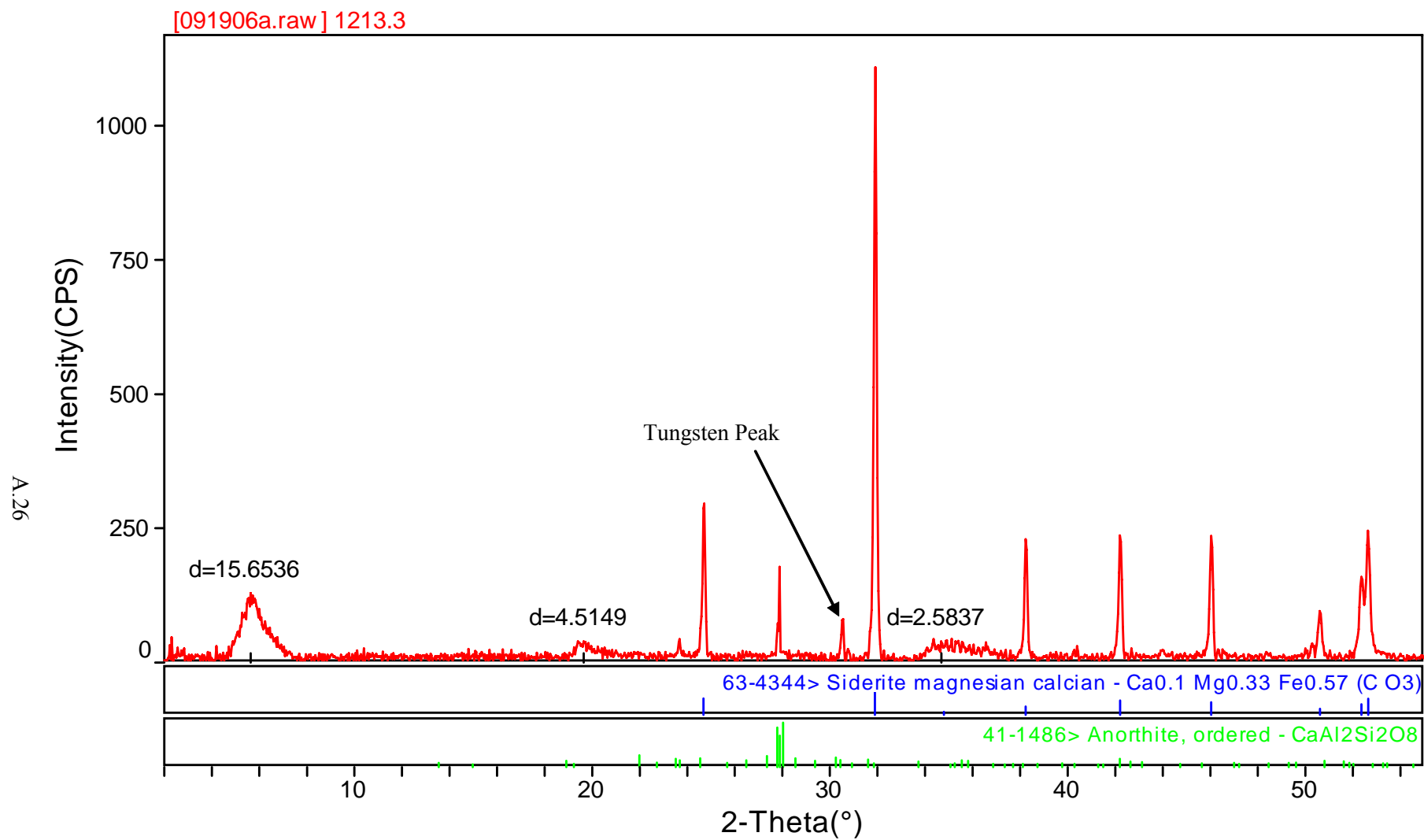


Figure A.26. XRD Pattern for Sample 1213.3

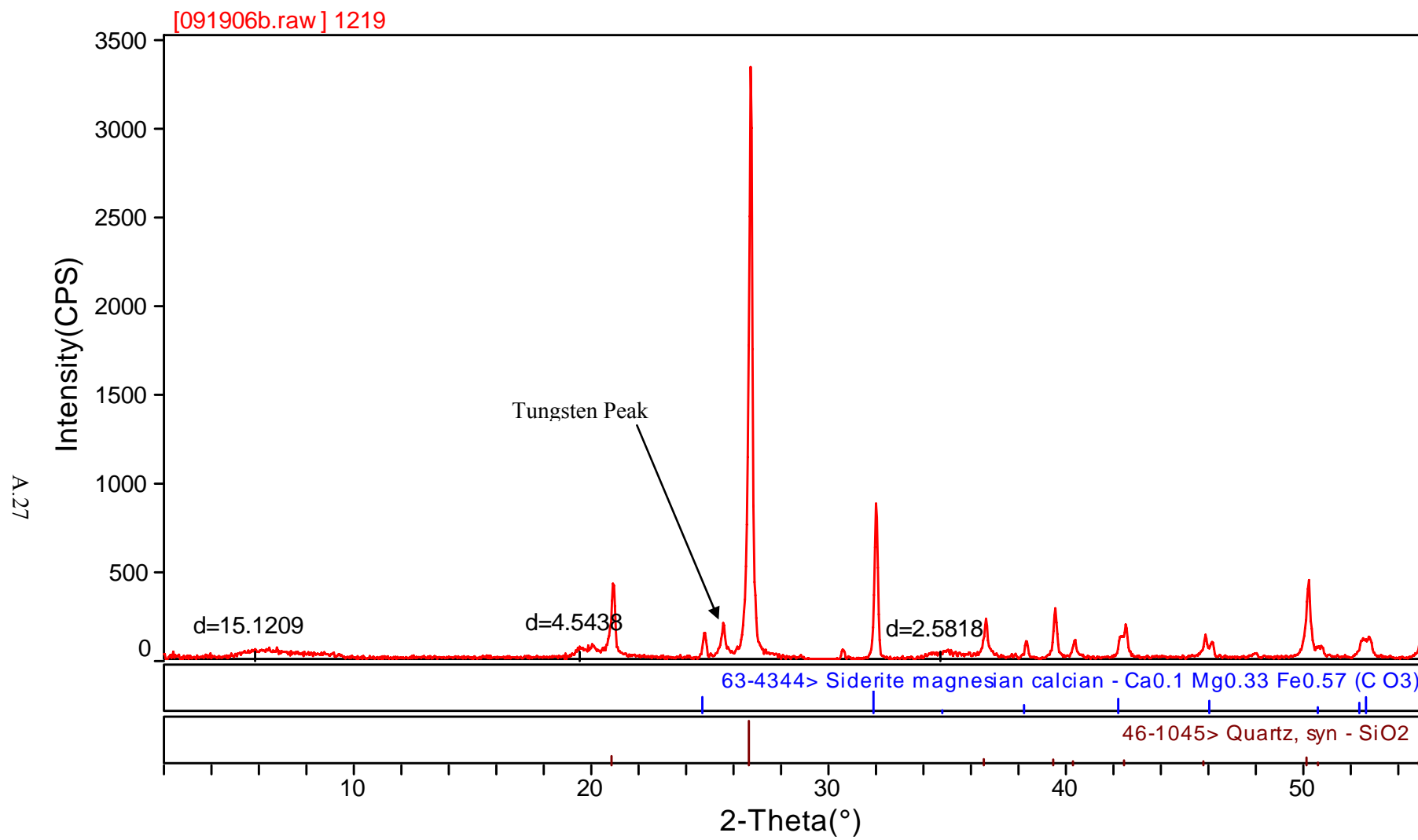


Figure A.27. XRD Pattern for Sample 1219

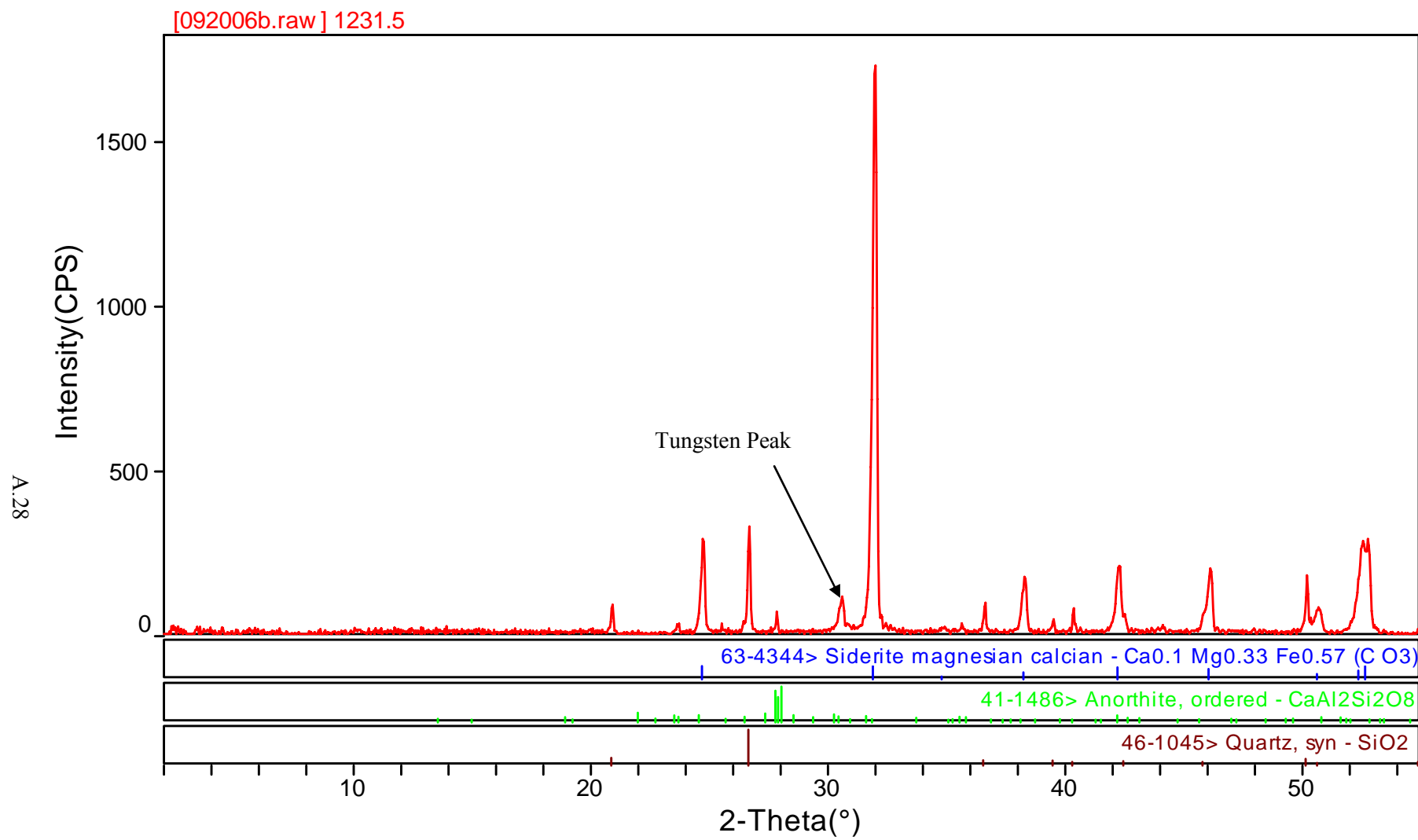


Figure A.28. XRD Pattern for Sample 1231.5

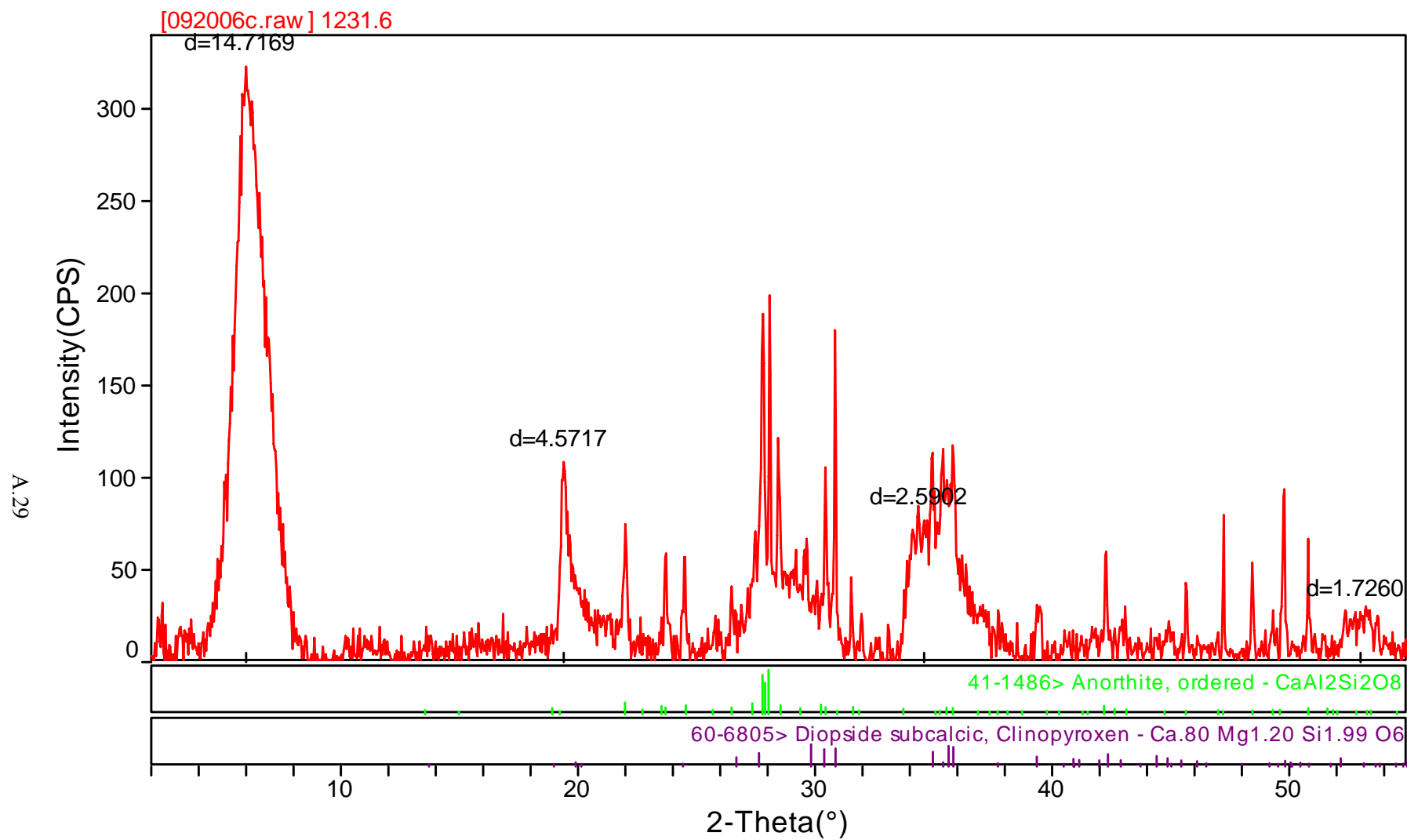


Figure A.29. XRD Pattern for Sample 1231.6

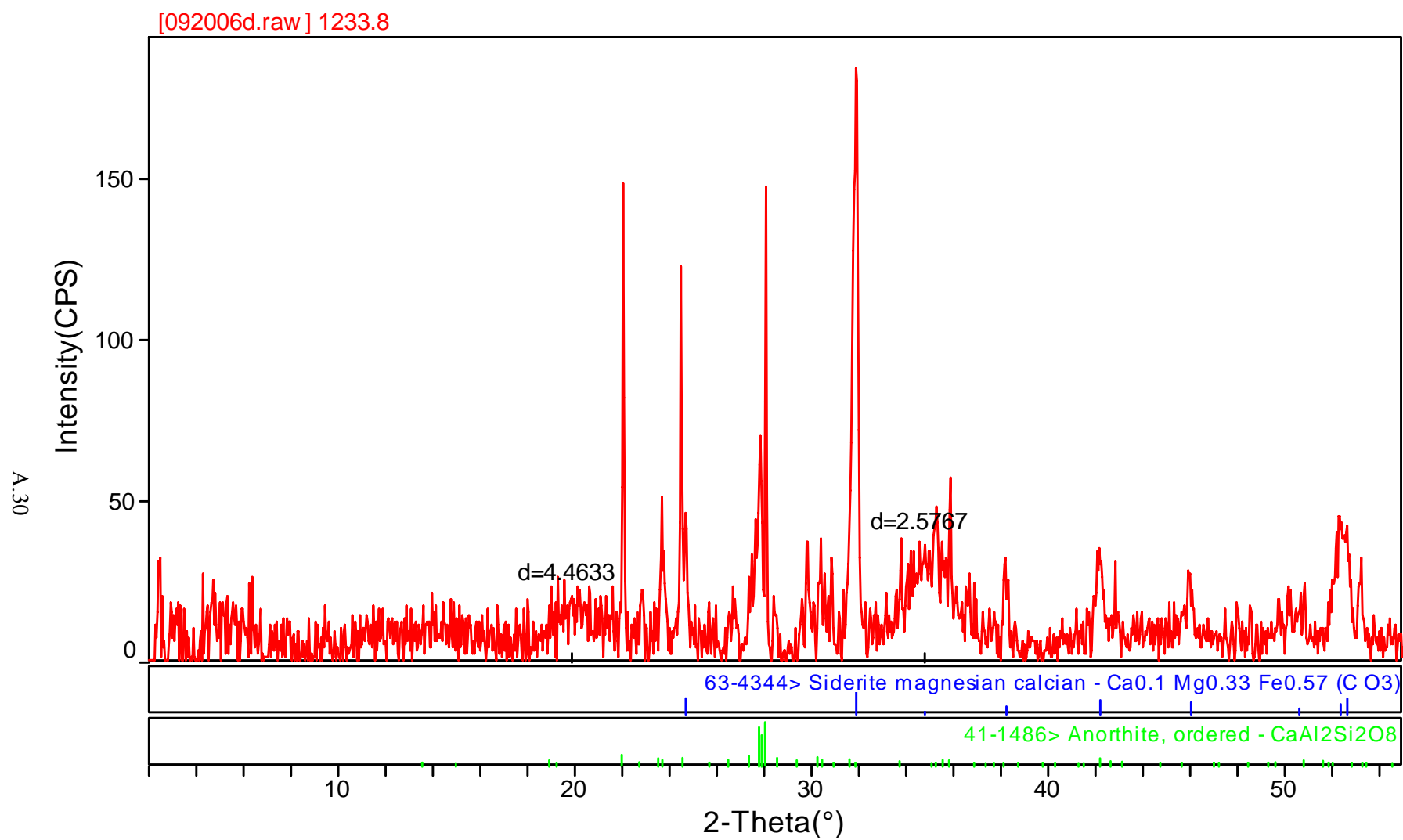


Figure A.30. XRD Pattern for Sample 1233.8

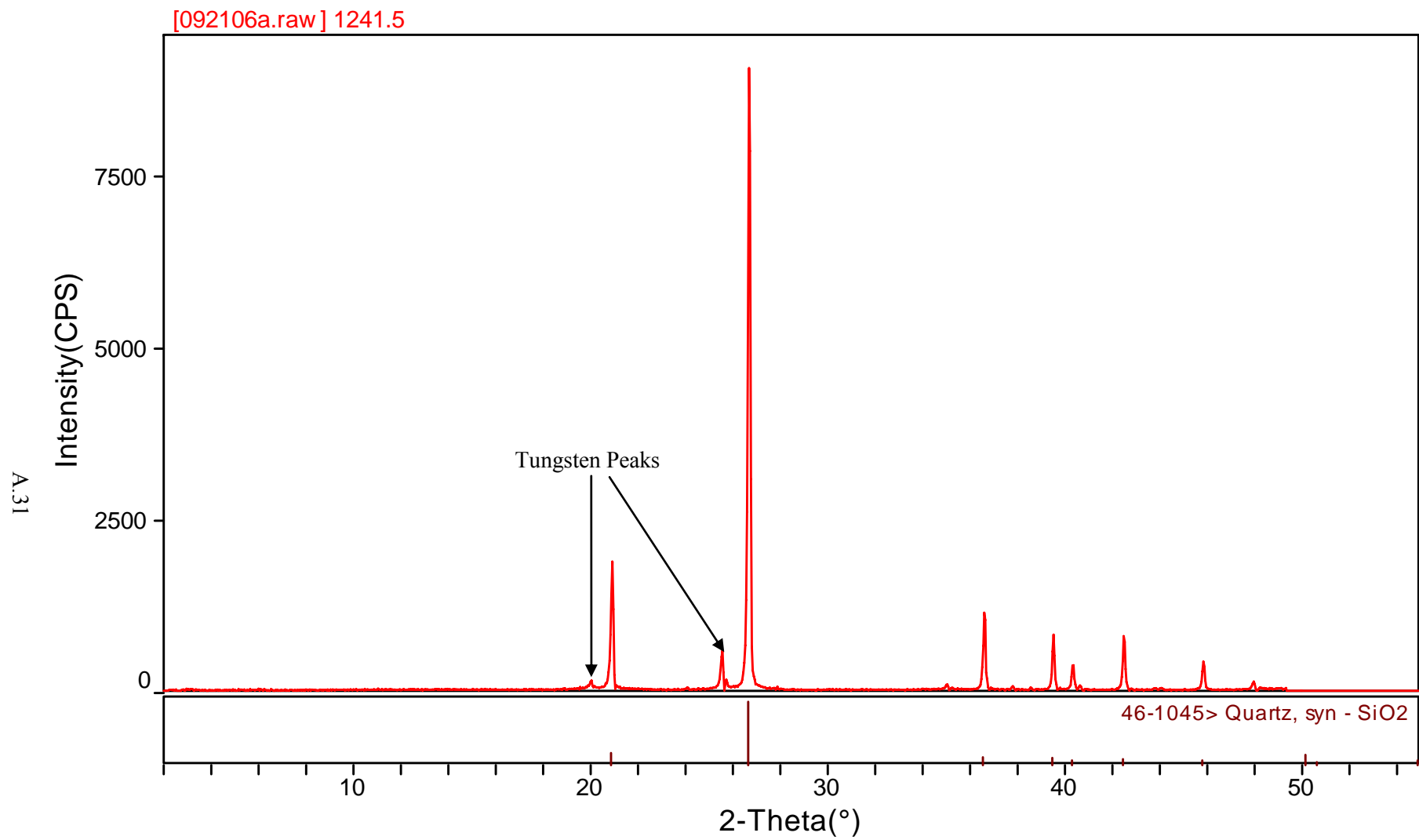


Figure A.31. XRD Pattern for Sample 1241.5

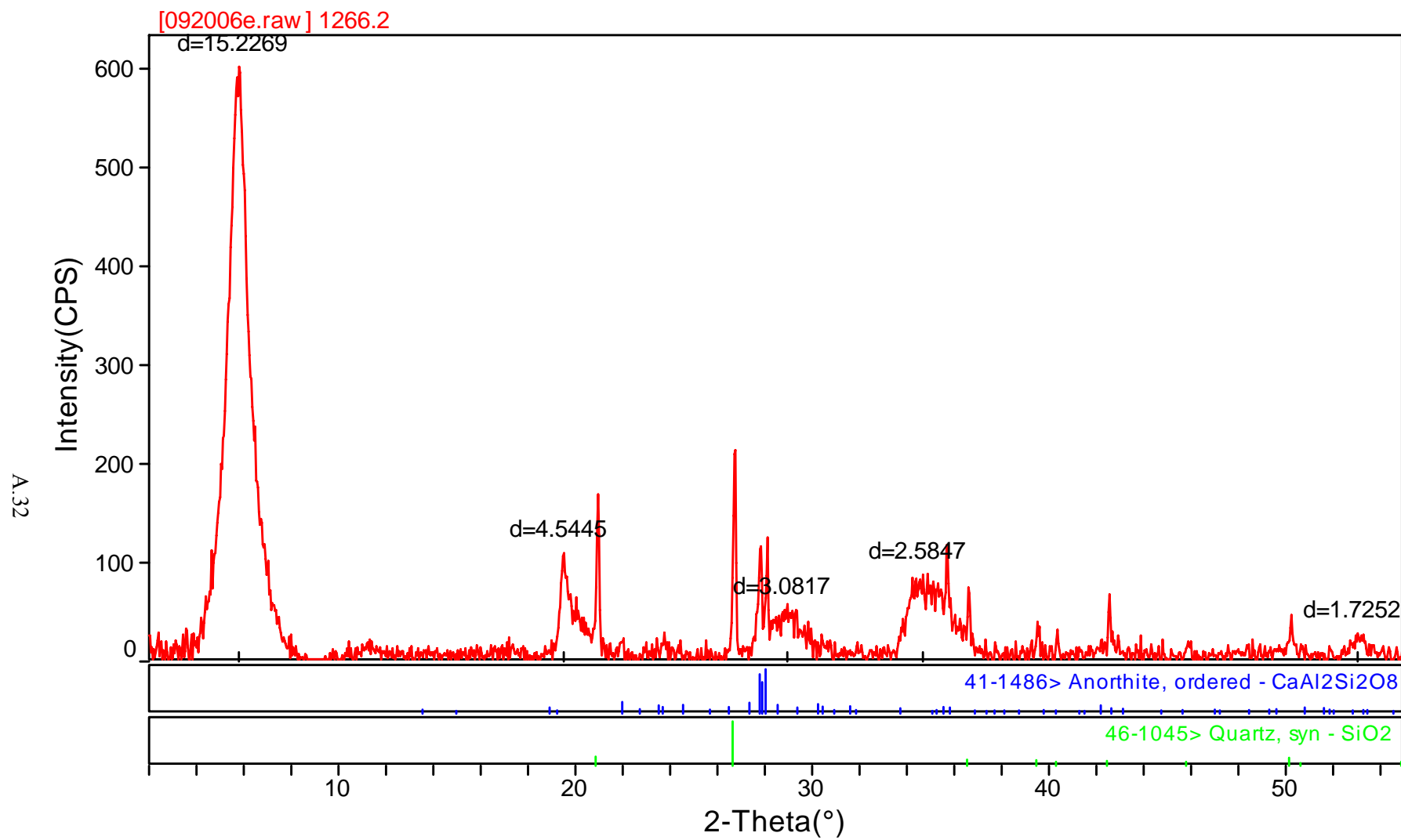


Figure A.32. XRD Pattern for Sample 1266.2

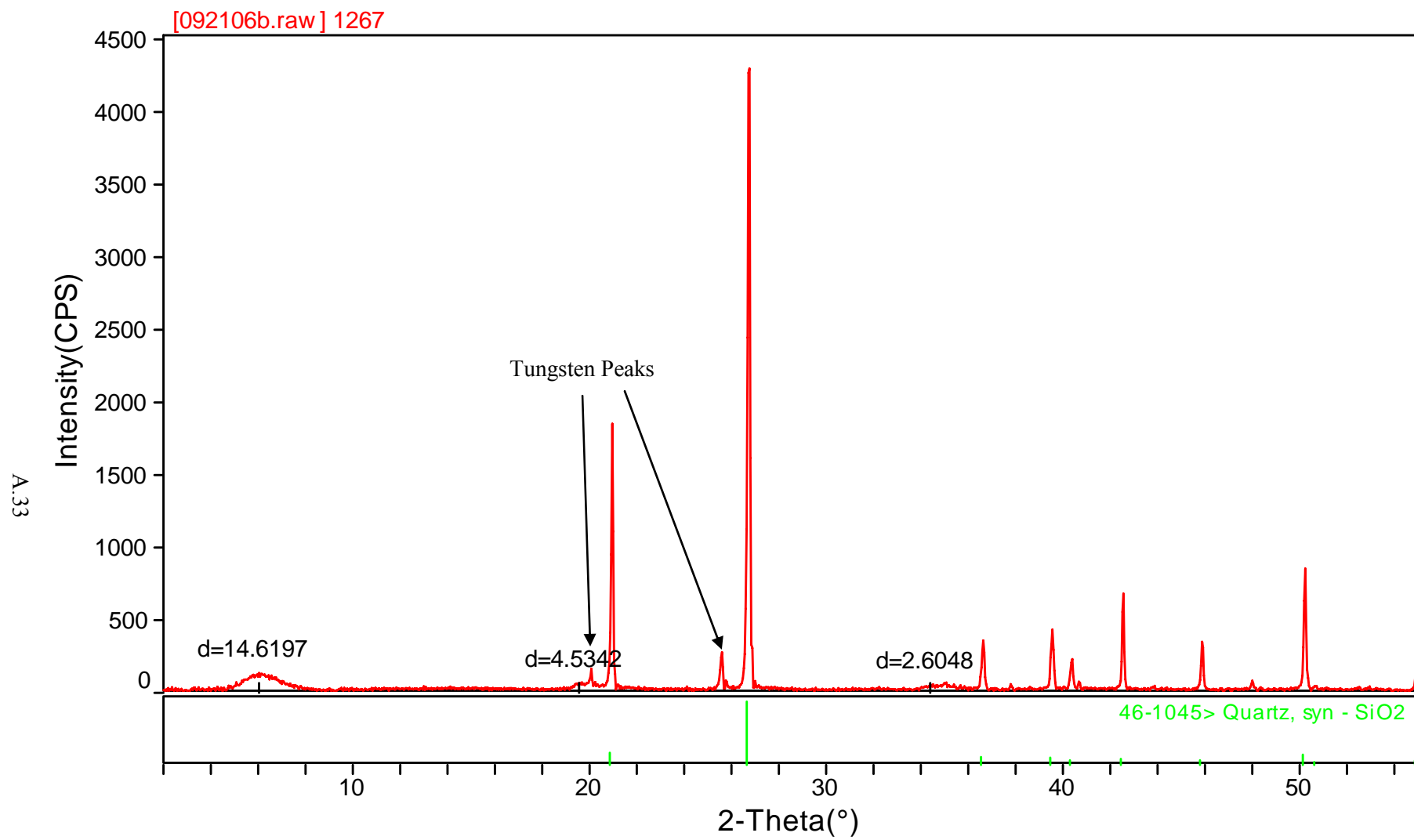


Figure A.33. XRD Pattern for Sample 1267

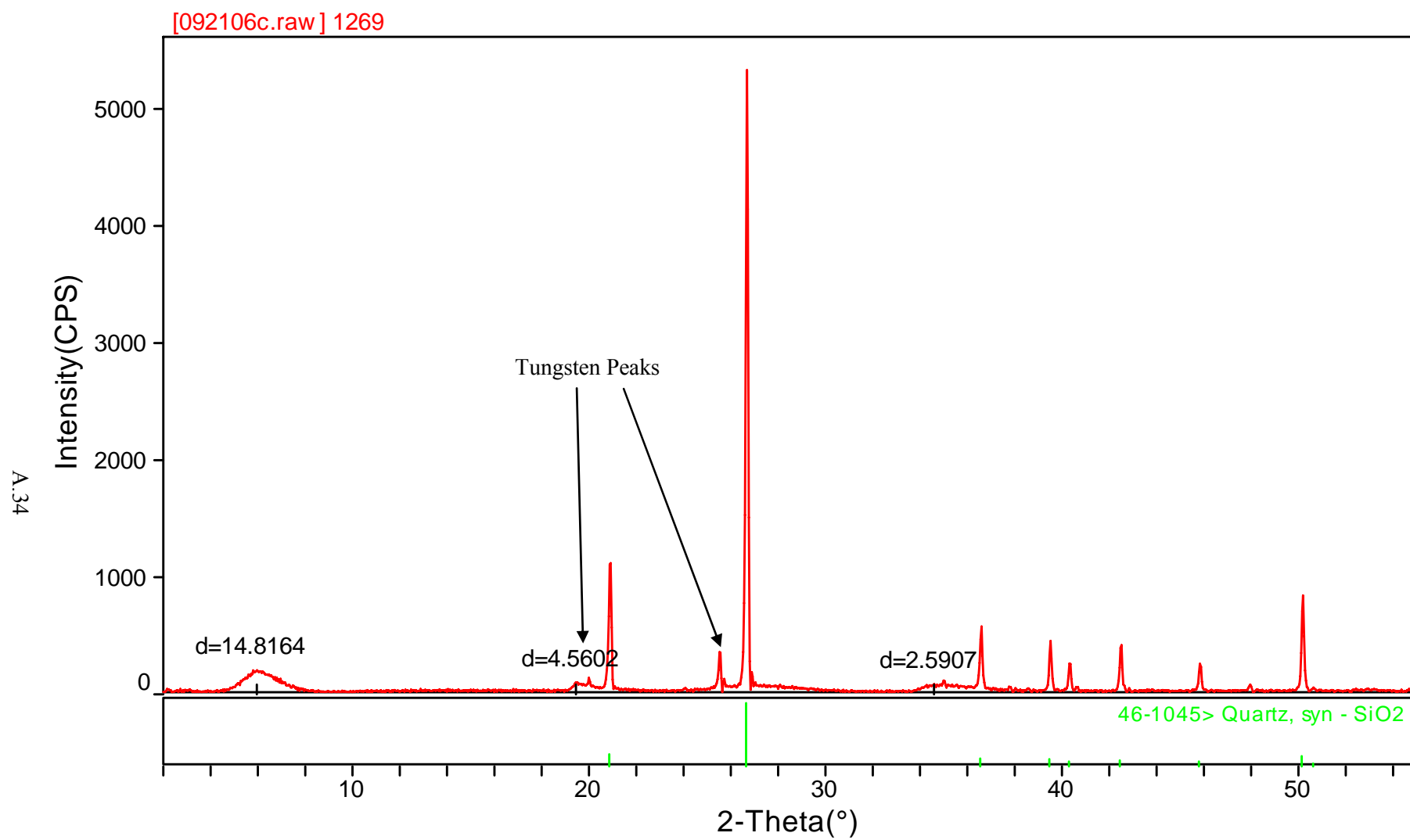


Figure A.34. XRD Pattern for Sample 1269

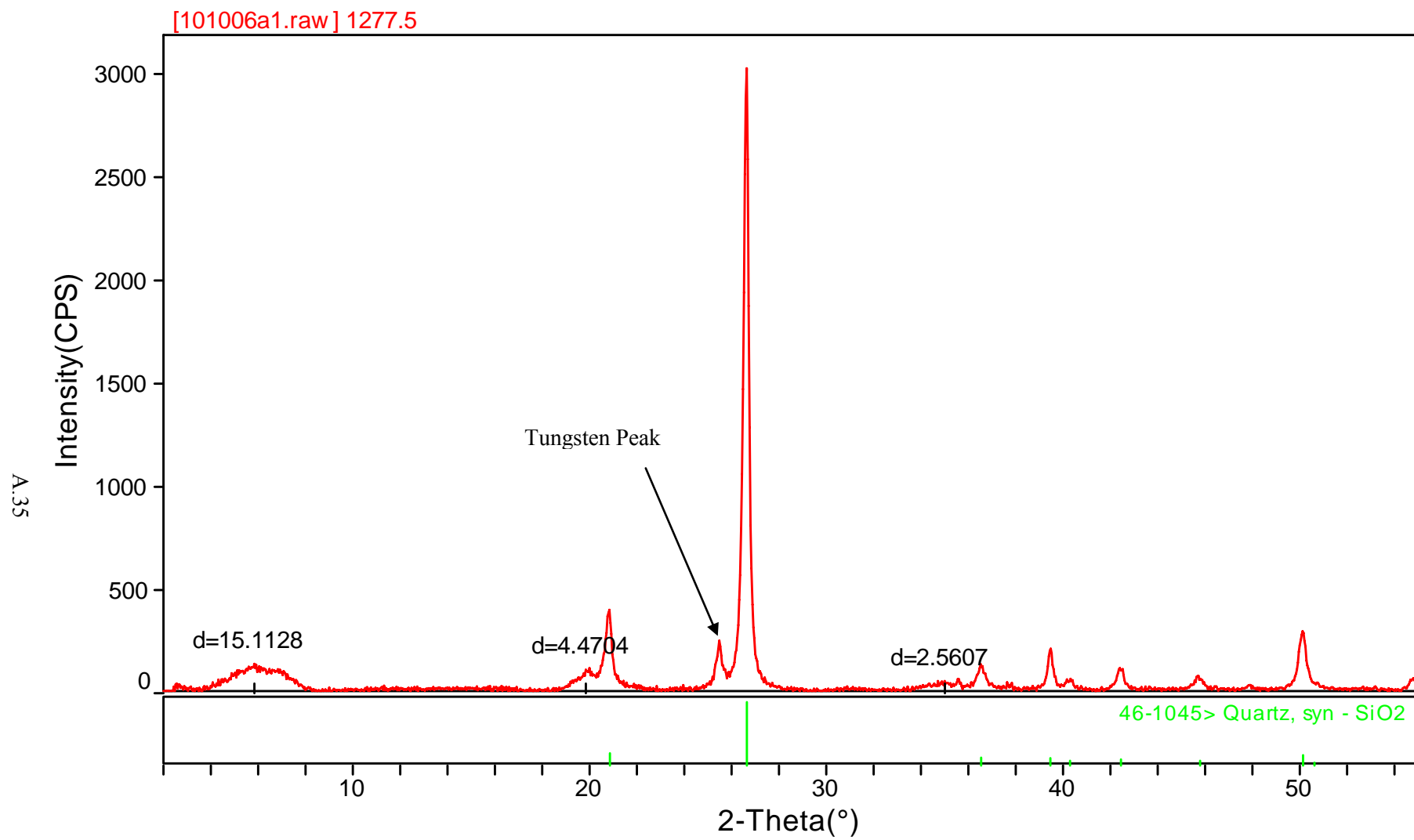


Figure A.35. XRD Pattern for Sample 1277.5

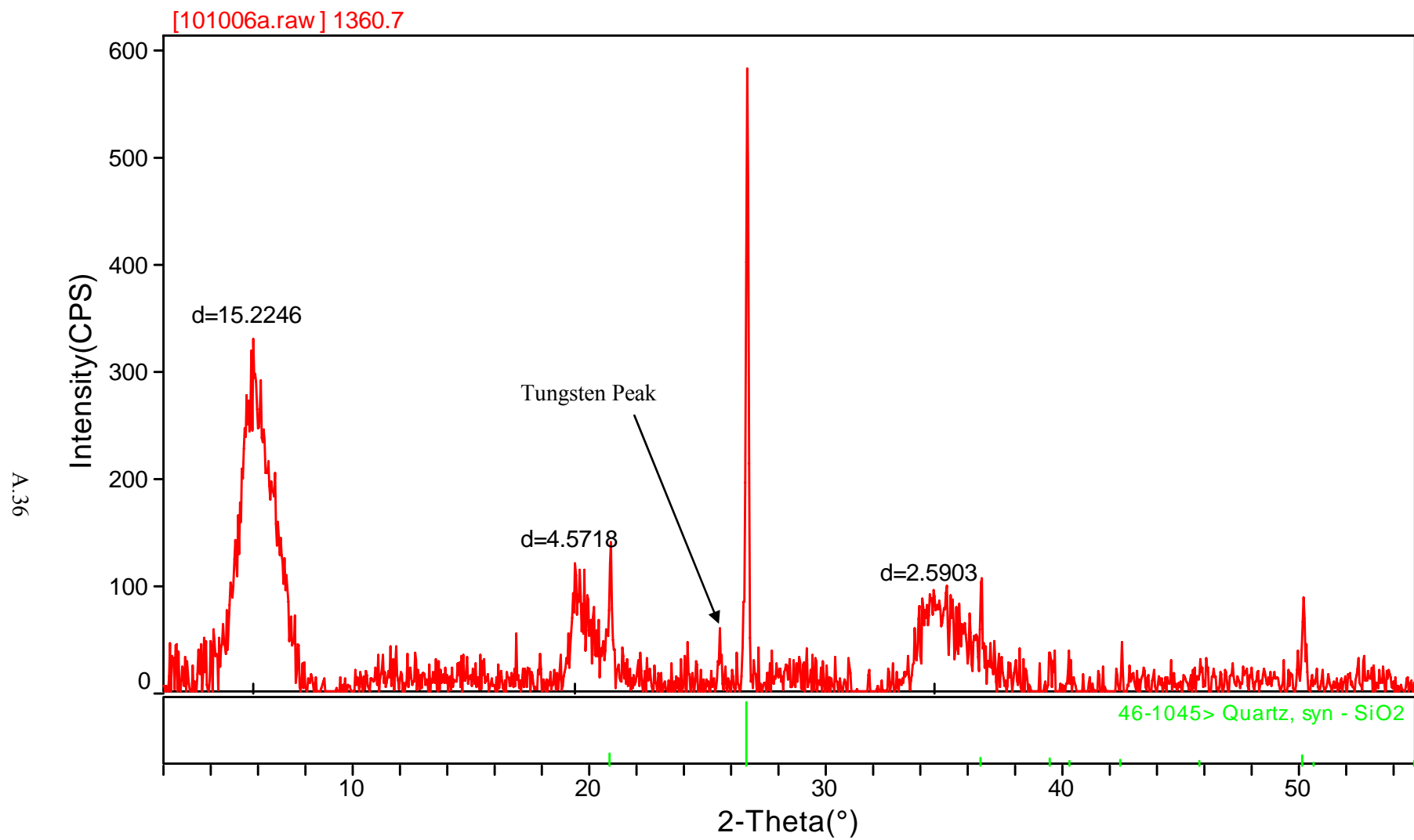


Figure A.36. XRD Pattern for Sample 1360.7

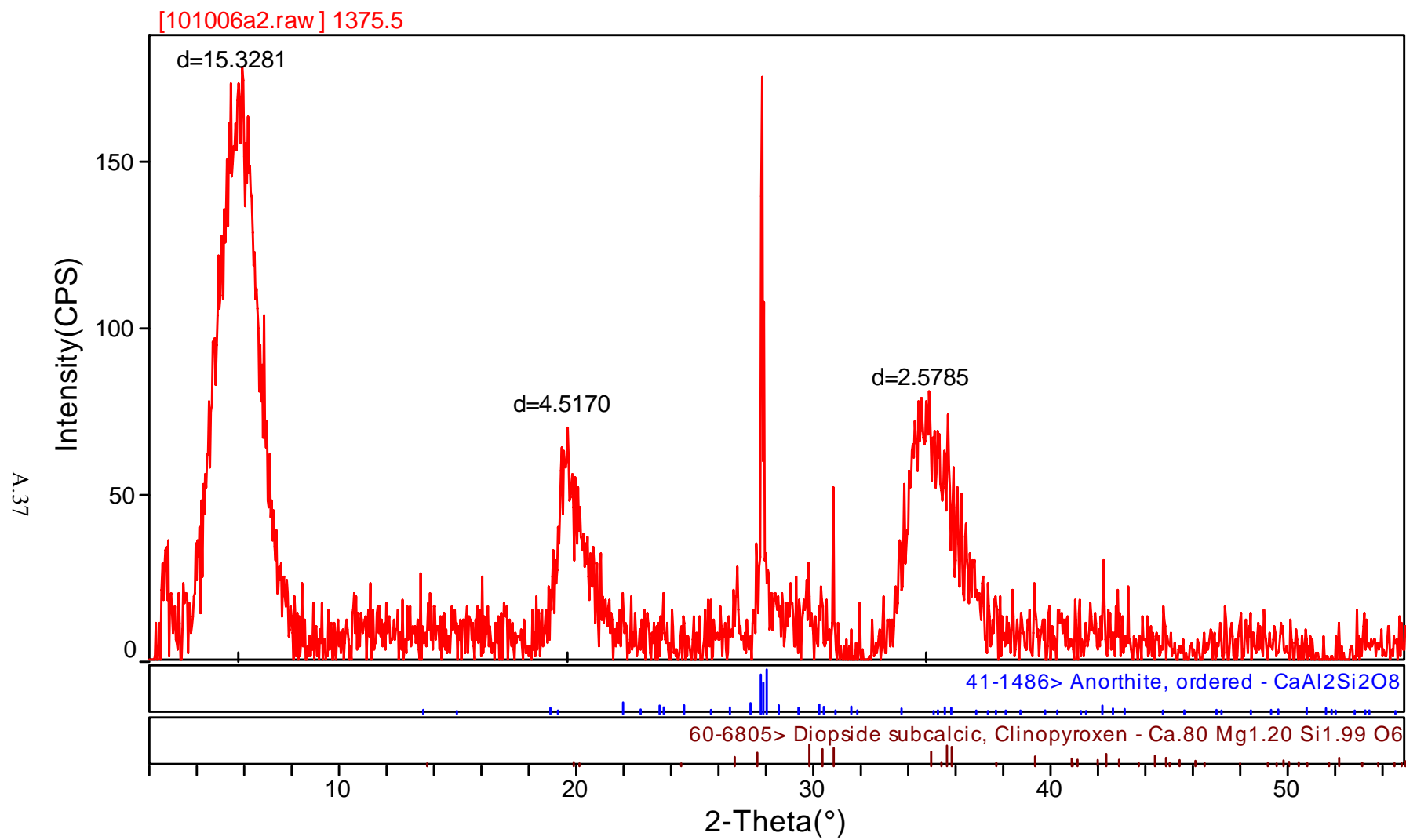


Figure A.37. XRD Pattern for Sample 1375.5